INTERFACIAL ELECTROCHEMISTRY

Theory, Experiment, and Applications

edited by

ANDRZEJ WIECKOWSKI
University of Illinois at Urbana-Champaign
Urbana, Illinois

MARCEL DEKKER, INC. NEW YORK · BASEL

ISBN: 0-8247-6000-x

This book is printed on acid-free paper.

Headquarters
Marcel Dekker, Inc.
270 Madison Avenue, New York, NY 10016
tel: 212-696-9000; fax: 212-685-4540

Eastern Hemisphere Distribution
Marcel Dekker AG
Hutgasse 4, Postfach 812, CH-4001 Basel, Switzerland
tel:41-61-261-8482; fax: 41-61-261-8896

World Wide Web
http://www.dekker.com

The publisher offers discounts on this book when ordered in bulk quantities. For more information, write to Special Sales/Professional Marketing at the headquarters address above.

Current printing (last digit):
10 9 8 7 6 5 4 3 2 1

PRINTED IN THE UNITED STATES OF AMERICA

33

Differential Electrochemical Mass Spectrometry as a Tool for Interfacial Studies

Helmut Baltruschat
University of Bonn, Bonn, Germany

ABSTRACT

Using an appropriate experimental setup, differential electrochemical mass spectrometry can be used to characterize submonolayer amounts of adsorbates on polycrystalline and single-crystal electrode surfaces by means of their desorption. One possibility to achieve this is to oxidize a carbonaceous species to CO_2, which is quantitatively detected in the mass spectrometer. Many adsorbates can also be desorbed at certain potentials as such or as the hydrogenated product, allowing a more direct characterization of the adsorbates. In some cases a nonreactive desorption can be induced by displacement with a second adsorbate, yielding additional information.

I. INTRODUCTION

In heterogeneous catalysis, one of the most often used techniques for the identification of adsorbates is thermodesorption mass spectrometry [1,2], which is sensitive enough to allow the detection of desorption products in the submonolayer range. It is used for the quantitative determination of adsorbate states, desorption products, surface reaction mechanisms (esp. by using isotope exchange reactions), and kinetic studies of the desorption reaction, including the determination of activation energies and the reaction order. Besides Kelvin probe measurements, it is probably the least expensive ultrahigh vacuum (UHV) technique.

Of course, this technique is not directly applicable to the solid phase–electrolyte interface. Not only is the mass spectrometric determination of species from an electrolyte more difficult (how to achieve this is one of the main topics of this chapter) but also desorption cannot be triggered by increasing the temperature due to the limited temperature range at least in aqueous systems. Luckily, desorption of many species can be achieved by applying an appropriate potential, which therefore replaces temperature as the variable.

Historically, the technique evolved out of the mass spectrometric determination of gaseous electrochemical reaction products as developed by Bruckenstein [3]. It was later improved by Wolter and Heitbaum [4,5] so that the time constant became short enough to allow the on-line detection of electrochemical reaction products, e.g., during cyclic voltammetry. Due to a proper design of the vacuum system, including two pumping stages, product formation rates were detected; to distinguish the technique from product sampling, i.e., integrating approaches, the method was called "differential." Even at the beginning it was sensitive enough to detect desorption products corresponding to about one monolayer of adsorbed species at porous electrodes.

In some respect, differential electrochemical mass spectrometry (DEMS) resembles the membrane introduction mass spectrometry [6]. This technique is used in analytical chemistry to detect trace amounts of nonpolar molecules in water; thin nonporous membranes (silicon or Teflon) are used to separate these molecules from water.

The nonporosity of the membranes has the advantage that much less water is reaching the vacuum; therefore, special pumping is not necessary. The drawback, however, is the relatively large response time of usually more than 10 s.

A review article on DEMS appeared in 1991 [7]. Therefore, after having described the technique, most examples deal with later developments.

II. INSTRUMENTATION

A. Teflon Membrane: Interface to the Vacuum

It is essential for DEMS to be able to separate the volatile products from the electrolyte. Fortunately, for aqueous systems and also for some organic electrolytes, e.g., propylene carbonate [8] and other solvents containing dimethylamine as constituent [9], this can be achieved by using porous Teflon membranes. Because of their hydrophobicity, the liquid does not penetrate through them, whereas dissolved gaseous and other volatile species readily evaporate in the pores.

The critical pore size for aqueous electrolytes depends on the surface tension of water and the contact angle between water and Teflon. It is calculated to be $r < 0.8$ μm [4]. The Teflon membrane is usually supported by a glass or steel frit.

A typical Teflon membrane (e.g., from Gore-Tex) is 75 μm thick and has a nominal pore width of 20 nm with a porosity of 50%. To achieve low time constants, the electrode has to be positioned very close to the membrane. One way to achieve this is to sputter the electrocatalyst layer, e.g., Pt, onto the Teflon membrane. The resulting catalyst layer typically has a thickness of 50–80 nm and a roughness factor between 5 and 10 (a simple model of such an electrode is shown in Fig. 1). Alternatively, as was done in the first DEMS experiments, a metallic lacquer (e.g., Doduco from Dürrwächter KG, Germany) containing small metallic particles can be painted onto the Teflon membrane. It has the advantage of a large roughness factor (50–100), permitting larger overall product formation. The disadvantage is the lower mechanical stability, and a much higher thickness (50 to 100 μm) leads to less well-defined diffusion behavior.

Other electrode types and electrochemical cells are discussed below; the common feature, however, is the Teflon membrane.

B. Vacuum System

Despite the hydrophobicity of the Teflon membrane, an appreciable amount of electrolyte evaporates. Because the flow is molecular within the pores, a value of $J' = 0.09$ mbar L s^{-1} cm^{-2} is calculated [4] for a porosity

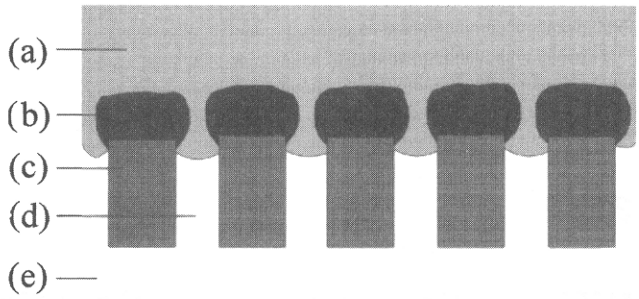

Figure 1 Schematic representation of a typical "sputtered" electrode. (a) Electrolyte, (b) catalyst sputter deposited, (c) Teflon, (d) pores in the membrane; and (e) vacuum.

of 0.5 and a vapor pressure for water of 23 mbar at 20°C, which corresponds to 0.25 mL of water per hour. The highest expected vapor pressure lies at around 100 mbar (water at 40°C), corresponding to a flow of $J' = 0.4$ mbar L s^{-1} cm^{-2}.

Under stationary conditions, this amount has to be pumped by the pumping system:

$$J' = p \times S \tag{1}$$

With an upper limit of 10^{-3} mbar in the ion source and a pumping speed S of 200 L s^{-1}, a flow of 0.2 mbar L S is allowed and therefore an electrode area of 0.5 cm^2 is acceptable.

The time constant τ for the detection of a species is directly given by the ratio of the ionization chamber volume V_0 (total volume of the chamber in which the ion source is situated; first pumping stage) to the pumping speed, as seen in the following: under nonstationary conditions, the change of pressure (e.g., after a sudden change of J') is given by

$$V_0 \mathrm{d}p/\mathrm{d}t = J' - p \times S \tag{2}$$

with the solution:

$$p = (J'/S) \times (1 - e^{-t/\tau}) \tag{3}$$

where $\tau = V_0/S$. With a pumping speed of 200 L/s and a volume V_0 of 1 L, a time constant of 5 ms is thus obtained, which is much less than the time constant attainable with the electrochemical cells (see below).

The analyzer section, of course, has to be pumped separately to achieve la pressure below 10^{-5} mbar. A 50-L/s turbomolecular pump is sufficient. Figure 2 shows a typical experimental setup. The electrochemical cell is connected to the first vacuum chamber via a valve at position 5. Another valve at position 6 leads to the calibration volume (see below). A shutter between the

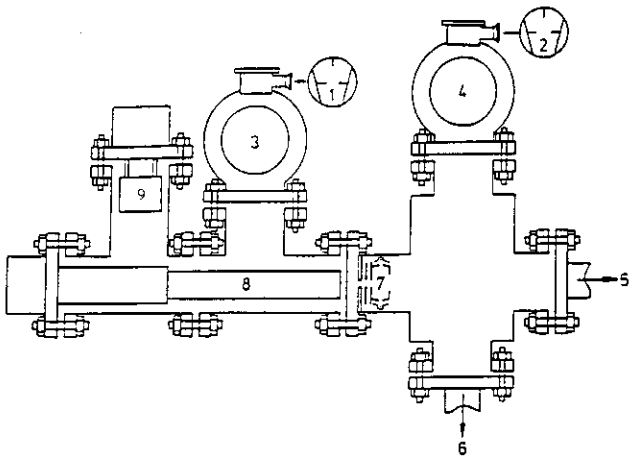

Figure 2 The vacuum system. 1 and 2, Rotary pumps; 3 and 4, turbomolecular pumps; 5, connection to the electrochemical cell; 6, connection to the calibration leak; 7, ion source; 8, quadrupol rods; 9, secondary electron multiplier. (From Ref. 44.)

ionization chamber and the analyzer section allows the difference in pressure. The secondary electron multiplier (10) is oriented 90° off axis, which has the advantage that light from the filament does not reach the multiplier. Higher stabilities are obtained using gas-tight ion sources, because the filament operates at a lower pressure than that existing in the ionization chamber.

The effort of pumping can be largely reduced by allowing a much higher pressure in the chamber of the first pumping stage of, e.g., 10^{-2} mbar and by simply pumping with a rotational pump at an accordingly lower pumping speed [10]. A sufficiently low time constant can easily be achieved by reducing its volume. In this case, the ion source has to be placed in a separate chamber that is pumped together with the analyzer of the mass spectrometer by a simple turbo molecular pump of 50 L/s. A commercial gas inlet system can be used. The disadvantage of such a system is that condensation or multilayer adsorption of the species might occur in that pressure range (cf. the vapor pressure of naphthalene, which is only 0.1 mbar at room temperature); heating of the gas inlet system may thus be necessary.

Product formation rates can be easily monitored by recording the corresponding ion current. The mass spectrometrically determined ion intensity I_i is directly proportional to the partial pressure p_i of that species i and therefore

$$I_i = ap_i = aJ_i'/S = \mathrm{RT}\, J_i a/S = K^\circ J_i \tag{4}$$

where a is a proportionality constant, $J_i = \mathrm{d}n/\mathrm{d}t = J_i'/\mathrm{RT}$ is the incoming flow in mol s^{-1}. K° thus contains all settings of the mass spectrometer and the ionization probability of the corresponding species.

When the species is produced electrochemically, J_i is given by the faradaic current I_F corresponding to that process:

$$J_i = N I_F/(z\,F) \tag{5}$$

where z is the number of electrons, F is the faraday constant, and N is the transfer efficiency, i.e., the ratio of the amount of the mass spectrometrically detected species to the total amount of species produced electrochemically. N may be less than 1 because a part of the produced species diffuses away from the electrode into the electrolyte. When the current efficiency is not equal to 100%, I_F has to be replaced by its product with the current efficiency. Therefore,

$$I_i = (K^*/z)I_F \tag{6}$$

with $K^* = K^\circ N/F$. Experimentally, both the low time constant of the vacuum setup of several ms and the proportionality of I_i with the faradaic current were verified [4,5].

Calibration of the mass spectrometer is achieved by connecting a separate calibration volume V_c to the first vacuum chamber via a calibration leak (e.g., a leak valve). The inflow rate J_i' is then given by the pressure decrease in the calibration volume $\mathrm{d}p_c/\mathrm{d}t$:

$$J_i' = V_c \mathrm{d}p_c/\mathrm{d}t \tag{7}$$

$$I_i = K^\circ J_i = K^\circ J_i'/\mathrm{RT} = (K^\circ/\mathrm{RT})V_c \mathrm{d}p_c/\mathrm{d}t \tag{8}$$

K° can thus be calculated from the pressure decrease in the calibration volume, i.e., from a plot of the ion current I_i vs the differentiated pressure p_c.

This calibration procedure cannot only be used for gases (most commonly CO_2) but also for volatile liquids. Special care, however, has to be taken that no adsorption or absorption occurs in a part of the calibration setup. Because of the limited linear range and a possible interference of the partial pressure of H_2O on the sensitivity, the same conditions as during the measurement should exist during calibration of the instrument. In particular, this means that during calibration, the electrochemical cell is connected to the vacuum system.

In some cases calibration is possible when using a known electrochemical reaction, such as hydrogen evolution. From Eq. (6), K^* and $N \cdot K^\circ$ are obtained

straight away. Often the oxidation of adsorbed CO on Pt electrodes is used to calibrate the mass spectrometer from CO_2. The integrated faradaic oxidation current and the integrated ion current for CO_2 have to be used. In this case, however, double-layer charging effects, which amount to 20% of the oxidation charge even after background substraction, have to be taken into account. The reason is the different double-layer charge at a given potential in the double-layer region with and without adsorbed CO and additionally the shift of the point of zero charge due to the adsorption of CO [5,11,12].

C. Cell Types

1. Conventional Cell for DEMS

The cell shown in Fig. 3 is optimized to have a low volume. This allows the use of expensive isotopically labeled compounds for mechanistic studies. In its first version, the cell body was made of Teflon; we now use glass because the porosity of the former sometimes leads to the absorbance of organic species.

The electrode has already been described in Chapter 1. It is mechanically supported by a steel frit. The response time for an electrochemical experiment was determined to be about 0.1 s [13], which is much larger than that of the vacuum system but still low enough for most electrochemical experiments.

A continuous forced convection may be achieved by simply introducing the electrolyte via a Teflon tube close to the electrode surface. When using volatile educts, it has to be kept in mind that due to evaporation, its concentration close to the surface of a sputtered electrode may be largely reduced, even when the electrochemical reaction is not diffusion limited. The electrochemical reaction (and also the adsorption process) and evaporation are competing processes. In the case of the thicker lacquer electrodes, the thickness of the porous electrode may be comparable with the thickness of the Nernstian diffusion layer (if the evaporation is diffusion limited) and the educt concentration may be different at the electrolyte side and at the Teflon membrane side of the porous electrode.

2. Cells with Defined Convection

Transport of species to the electrode can be largely accelerated and also better defined by using rotating electrodes. In some cases it might therefore be interesting to use a rotating porous electrode as an inlet system to the mass spectrometer as it was described [14].

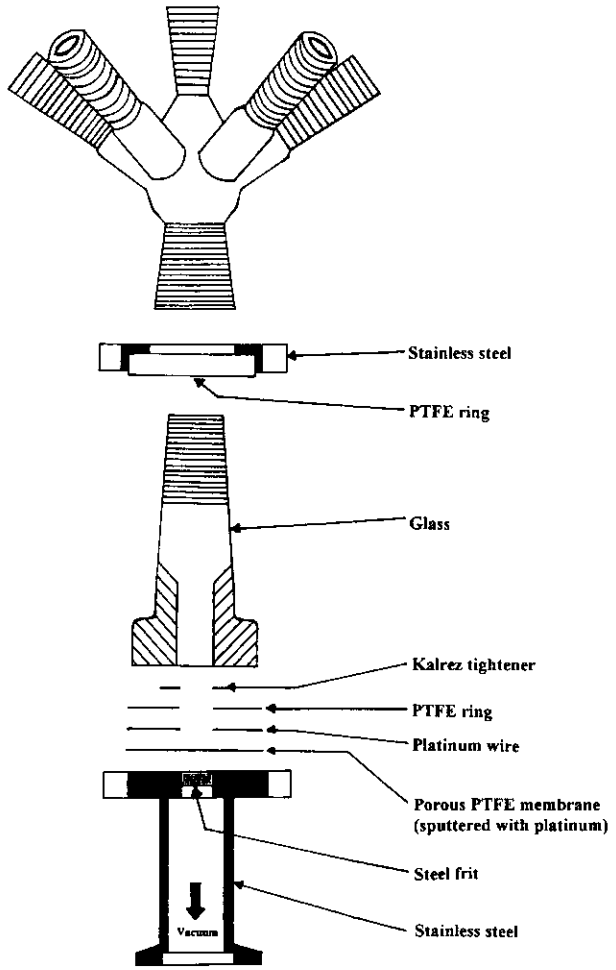

Figure 3 The conventional cell for DEMS.

Using such a rotating inlet system, the transfer efficiency N can be determined under defined diffusion conditions from a plot of the diffusion limited faradaic currents from hydrogen evolution vs. the corresponding values of I_i for different rotation speeds.

Using sputtered platinum electrodes, a transfer efficiency above 0.9 was obtained even at high rotation speeds. Obviously, in the whole range of rotation speeds the concentration gradient across the catalyst layer is much larger than the concentration gradient away from the electrode into the bulk electrolyte, with a correspondingly large Nernstain diffusion layer (cf. Fig. 4). Using lacquer electrodes 50 to 100 μm thick, the transfer efficiency only approached 0.7 at low rotation speeds and was 0.3 at high rotation speeds. Here, the diffusion layer from the surface of the electrode to the Teflon membrane is comparable with the diffusion layer in the bulk electrolyte.

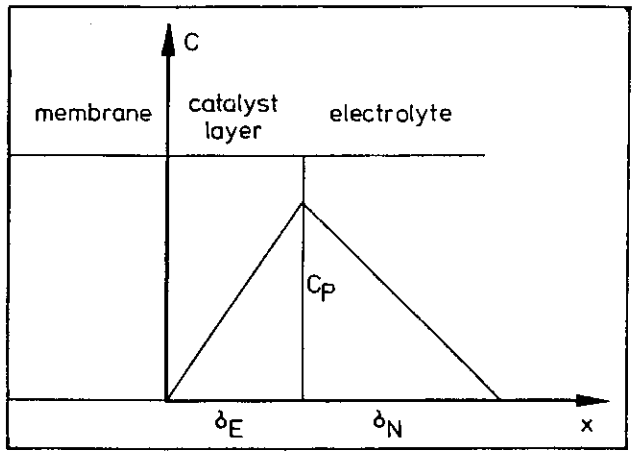

Figure 4 Product concentration profile. δ_E, Thickness of the electrode; δ_N, diffusion layer thickness. (From Ref. 14.)

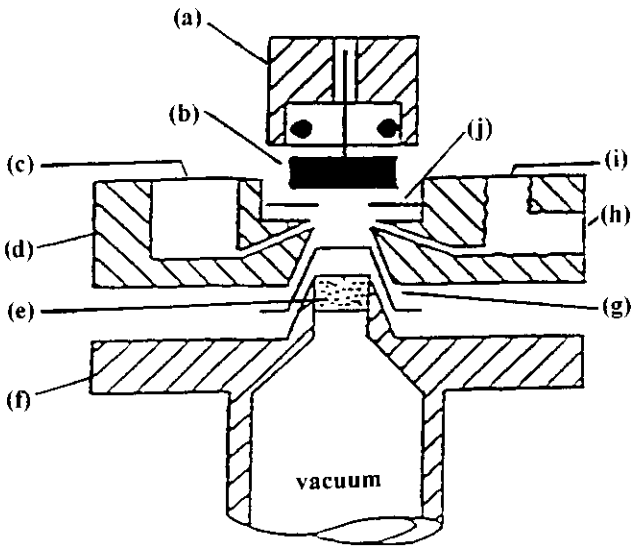

Figure 5 Thin-layer cell. (a) Electrode holder; (b) single-crystal electrode; (c) connection to reference electrode, second counter electrode, and electrolyte outlet; (d) cell body made from titanium; (e) steel frit; (f) stainless steel support; (g) microporous Teflon foil, interface between electrochemical cell and vacuum; (h) connection to counter electrode; (i) electrolyte inlet via needle valve; (j) Teflon spacer, 50–100 μm thickness; inner diameter 6 mm. (From Ref. 16.)

The situation is somewhat different when the transfer efficiency for the desorption products of an adsorbate layer is considered. For the case of a fully covered electrode, the product is formed evenly distributed within the catalyst layer, including the pores (and not only formed at the macroscopic surface). Therefore, for carbon dioxide formation from adsorbed CO on Pt, transfer efficiencies slightly above 0.5 were found for the lacquer electrode even at high rotation speeds, whereas the transfer efficiency for the sputtered electrode still was around 0.9.

To avoid the technically demanding rotational feed-through into the vacuum, a much simpler approach was described [15]. Here, a cylinder made up of an inert material rotates approximately 5 mm above the stationary porous electrode. Defined mass transfer to the electrode is achieved by the rotational flow.

3. Cell Types Allowing the Use of Massive Electrodes

To be able to use massive electrodes, e.g., single-crystal electrodes for DEMS, the thin layer cell of Fig. 5 was constructed [16,17]. The massive electrode with a diameter of 1 cm is separated from the porous hydrophobic Teflon membrane by a 50- to 100-μm-thick electrolyte layer. Volatile species produced at the electrode surface diffuse to the Teflon membrane within 2 s. The Teflon membrane (75 μm thick, pore width 0.02 μm, porosity 50%) is mechanically supported by a steel frit. The distance between electrode and Teflon membrane is ascertained by a spacer (or two to achieve a doubled distance; ID, 6 mm; OD, 12 mm) made from the same Teflon membrane. Because of compression of this soft spacer, the distance is less than the nominal thickness.

The cell body is made out of passivated titanium because of its mechanical stability and inertness (the passivating procedure has to be repeated from time to time). Attempts to use Kel-F were not successful due to its hydrophobicity, which leads to the formation of gas bubbles in the capillaries (or at the junction between capillaries and the Teflon membrane or spacers).

Two capillaries positioned at opposite sides serve as electrolyte inlet and outlet and as a connection to the reference and counter electrode. Because of the large ohmic potential drop (product of current and electrolyte resistance) in the thin layer of electrolyte, it is advantageous to use two counterelectrodes both in the outlet and inlet. By connecting both counterelectrodes to the potentiostat via different resistors, the total current is divided into two parts such that the current through the capillary to the reference electrode is much less than 50% of the total current. Connecting some current flow through the capillary to the reference electrode also leads to a much higher electronic stability. Potential oscillations may occur otherwise.

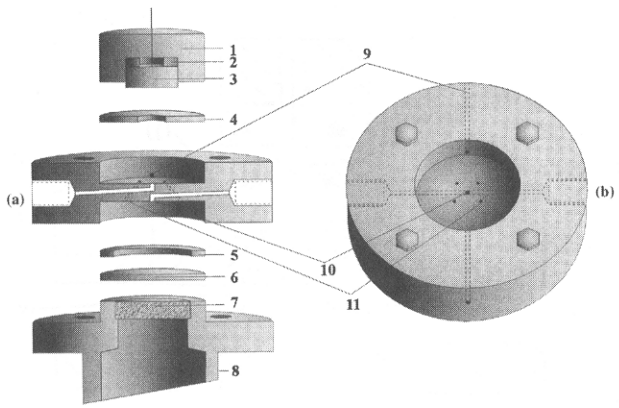

Figure 6 Dual thin-layer cell from experiments under constant flow through (Kel-F). 1, Kel-F support; 2, Kalrez tightener; 3, single crystal; 4 and 5, Teflon tighteners; 6, porous Teflon membrane; 7, stainless steel frit; 8, stainless steel connection to the vacuum system and the mass spectrometer; 9, capillaries for flushing with Ar; 10, inlet–outlet capillaries; 11, connecting capillaries. (a) Side view of Kel-F body of the cell; (b) top view of the cell.

This cell can be used for both desorption experiments under stopped flow conditions and for the measurements of product formation rates during faradaic reactions under continuous flow. In the first case, nearly all of the desorption product can diffuse within 2 s to the Teflon membrane, where it evaporates. (Experimentally, we obtained transfer efficiencies N in the range of 0.9–0.95 [18].) During a continuous flow of electrolyte, however, a considerable part of the product is transported out of the thin-layer volume and lost, because a part of the product is formed close to the outlet of the cell and has no chance to reach the Teflon membrane. Experimentally, transfer efficiencies of 0.2 and below for practical flow rates of 1 μL/s and above were found [19].

Better suited for faradaic reactions, which have to be performed under a continuous flow of electrolyte on account of the rapid depletion of the reactant in the thin-layer cell, is the "dual thin-layer cell," shown in Fig. 6. Here, the complete cell consists of two separate compartments for the electrochemistry and the mass spectrometric detection. The electrolyte first enters the thin-layer compartment in front of the electrode ("wall-jet" geometry) and then flows through four capillaries into the lower compartment, where volatile products can reach the Teflon membrane. This cell offers the additional advantage that it can be combined with a quartz crystal microbalance; then, one of the electrodes of the quartz is also used as a working electrode for DEMS [20].

To test the applicability of DEMS for various substances, an aqueous solution of test analytes was delivered to the cell and the mass spectrometric ion current was recorded as a function of the flow rate $u = dV/dt$ and, after calibration of the mass spectrometer, converted to flux J through the membrane (Fig. 7a; the working electrode was replaced by a glass dummy). The straight line corresponds to the assumption of complete turnover of the incoming species. As expected, sensitivity as given by the ratio J/c is highest for gases and lowest for hydrophilic substances. Obviously, the transfer of

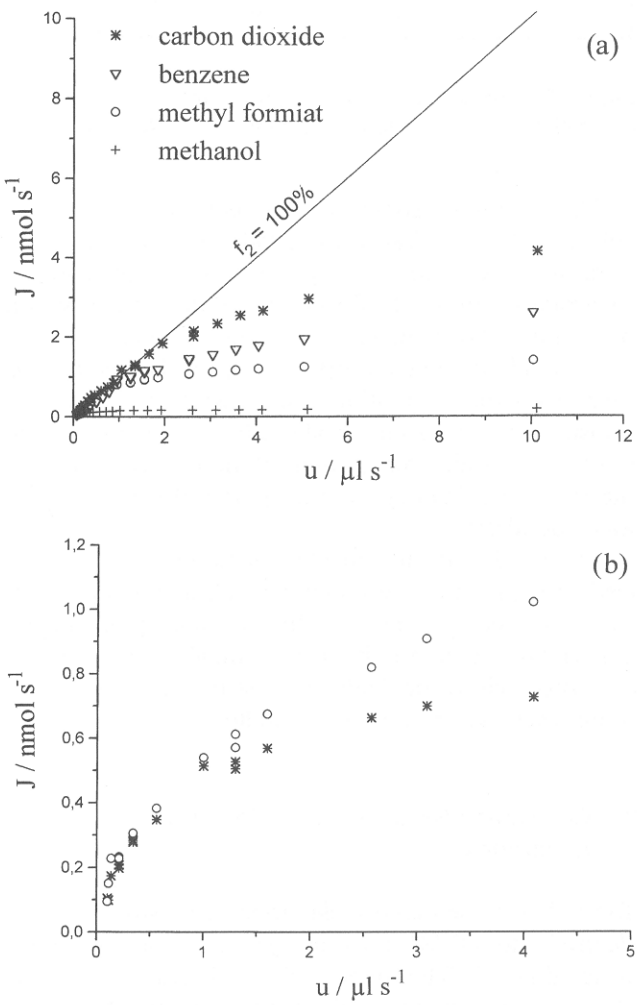

Figure 7 Performance of the dual thin-layer cell. (a) Ion currents converted to flux and normalized by the concentration (CO_2; 38 mM; benzene, 23 mM; formic acid methylester, 2 mM; methanol; 2 mM). (b) Plot of the faradaic current of CO oxidation at Pt (○) and the corresponding mass signal for CO_2 (∗), both converted to the flux J; 0.5 M H_2SO_4 saturated by CO. $E = 1$ V.

soluble species is not diffusion limited. Under identical conditions, benzene was even detected at concentrations of 1 μM, demonstrating the high sensitivity of the technique.

In electrochemical thin-layer flow cells, the faradaic current is proportional to u^x with $x = 1/3$ for diffusion limited processes, as long as the flow rate $u = dV/dt$ is not so small that most of the incoming species reacts at the electrode surface. In the latter case, I_F is proportional to the amount of species entering the cell and therefore to u^1. The same proportionality should hold for the ion current. However, a logarithmic plot of the data gives a value of 0.6 for x in the case of CO_2 and also Ar, which might reflect a certain similarity of the cell to wall-jet cells, for which $x = 3/4$.

The collection efficiency f_1 is the ratio of reacting species [given by $I_F/(z \times F)$] to the amount of species entering the cell compartment:

$$f_1 = I_F/(zF \times c \times u) \tag{9}$$

Similarly, the collection efficiency for the mass spectrometric part of the cell is given by

$$f_2 = I_i/(K_0 \times c_p \times u) \tag{10}$$

This value can be obtained from Fig. 7a by forming the ratio between the experimental value and the value given by the straight line. In an electrochemical experiment, the concentration of the product in the fluid leaving the electrochemical part of the cell is given by

$$c_p = I_F/(zF \times u) \tag{11}$$

Therefore,

$$I_i = f_2 K_0 I_F/(zF) = N K_0 I_F/(zF) \tag{12}$$

and the collection efficiency of the "detection" cell f_2 is identical to the transfer efficiency N as defined in Eq. (5). This is not the case for the cell depicted in Fig. 5! A plot of the faradaic current of CO oxidation at Pt and the corresponding mass signal for CO_2, both converted to the flux J, is shown in Fig. 7b. Collection efficiencies, as given by the ratio of mass spectrometric to the faradaic current signal, are close to those expected from Fig. 7a. This and their high values approaching 1 at low flow rates confirm the suitability of this cell for quantitative measurements.

A simpler approach, also allowing the use of massive electrodes, was previously described [21]. Here, the gas inlet is a pinhole, several micrometers in diameter, located at the hemispherical end of a glass tube, 4 mm in diameter, which is covered by a Teflon film of 50 μm. Electrodes can be used in the hanging meniscus arrangement. A further advantage is the small overall amount of substance entering the vacuum system via the pinhole. However, a disadvantage seems to be that the volatile products are sampled not only from a small cylindrical volume between the pinhole and the electrode surface in front of the pinhole but from a larger volume. The superposition of the products' planar diffusion away from the surface and the spherical diffusion to the pinhole leads to a complicated time dependence and larger response times.

A rotating rod in front of the porous Teflon membrane was also used as a massive electrode [22]. The use of single crystals, however, makes no sense, and mass transfer and transfer efficiency are less defined than in the thin-layer cells and the rotational flow cell described above.

The study of single crystals under illumination is also possible using the cell of Fig. 8 [23]. Here, volatile products diffuse sideways through the ring made out of a Teflon membrane. Because of the large response time, low scan rates of 2 mV/s have to be used.

III. CHARACTERIZATION OF ORGANIC ADSORBATES

Organic adsorbates play an important role not only as intermediates in electrocatalytic reactions but also as inhibitors of corrosion and brighteners in metal plating. When studying these adsorbates, the fundamental questions are as follows:

Is the adsorption associative or dissociative, i.e., does bond breaking occur upon adsorption?
What is the exact orientation and composition of the adsorbate?
How stable is the adsorbate and how does the coverage depend on concentration and potential?
Which are the desorption reactions?
What is the influence of the atomic structure?

In the following, it is shown that DEMS is a versatile method in finding answers to these questions.

With DEMS, adsorbates can be characterized by determining the amount and nature of desorbing species. Desorption can be induced either by displacement by other adsorbates, such as adsorbed hydrogen or underpotential deposition (UPD) of Cu, or by a reactive desorption, such as oxidation or hydrogenation. Examples presented here focus on work done with single-crystal electrodes and the effect of single-crystal orientation.

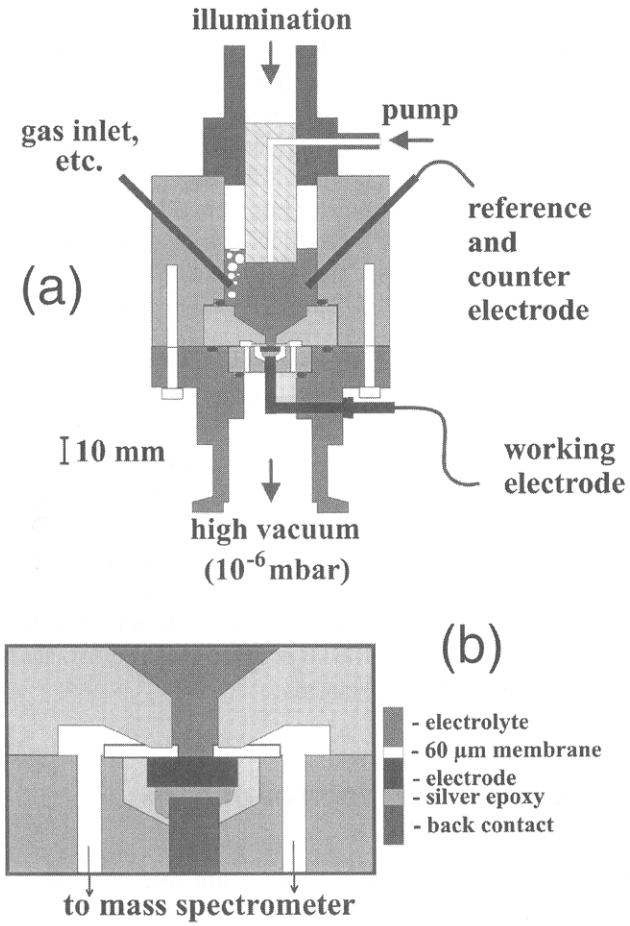

Figure 8 A DEMS cell for using massive electrodes under illumination. (a) Schematic drawing of the cell. (b) Detail of the inlet system. (From Ref. 23.)

A. Benzene

Benzene is an ideal model compound to study adsorption on Pt electrodes and the versatility of DEMS for two reasons: it adsorbs quickly and irreversibly and the molecule is stable enough to stay intact upon adsorption and not to break apart and lead to a variety of adsorbed species, as is the case for, e.g., ethene (see below).

The typical experimental procedure for studying adsorbates is as follows. After annealing, the cleanliness of the single crystal is checked by cyclic voltammetry in the supporting electrolyte, e.g., sulfuric acid. The crystal is then transferred to the DEMS cell (Fig. 5), its surface being protected by a droplet of electrolyte. After having again been checked for cleanliness by cyclic voltammetry and, sometimes, holding the potential at −50 mV to achieve desorption of possible contaminants, the new electrolyte containing the adsorbates (e.g., benzene) is flushed through the cell (typically 1 mL at a flow rate of 20 μL/s) at a fixed potential in the double-layer region. After an electrolyte exchange with the supporting electrolyte (still at the same potential), a potential sweep is started to induce reactive or nonreactive desorption.

The cyclic voltammogram and the corresponding mass spectrometric cyclic voltammogram (MSCV) for CO_2 during the oxidation of the benzene preadsorbed at a Pt(111) electrode are shown in Fig. 9 [24].

Oxidation proceeds in two well-separated steps. The MSCV shows that no CO_2 is formed during the first peak but only during the second one. Complementary experiments in an H cell have shown that the adsorbate is not desorbed after the first peak. The CO_2 detected in the second peak is the only detectable oxidation product. As shown by the ion current for CO_2 in the second and third sweep, complete oxidation of the adsorbate is not achieved in the first cycle. From an integration of the ion current over the three sweeps, the total amount of CO_2, and therefore the total benzene coverage, can be calculated. A coverage of 0.26 nmol/cm^2 is obtained. The charge in the first oxidation peak amounts to one fourth of the total oxidation charge. Because oxidation of benzene to benzoquinone requires the release of 6 electrons or one fifth of the 30 electrons corresponding to the complete oxidation to CO_2, it is probable that adsorbed quinone is formed as an intermediate, according to

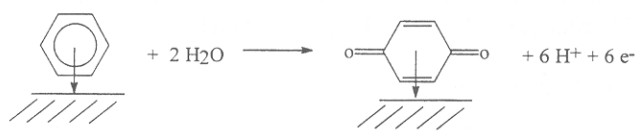

(13)

The oxidation of adsorbed benzene on Pt(110) and Pt(100) and also on a roughened Pt(111) electrode is very similar to that on a polycrystalline electrode and only occurs in the oxygen adsorption region, leading to CO_2 [24,25]. The faradaic current and the ion current can be used to determine the coverage of the electrode with benzene. A comparison of the faradaic oxidation charge with the integrated ion current indicates five electrons per formed CO_2 molecule consistent with complete oxidation to CO_2. When oxidation charges are evaluated separately for the first and subsequent sweeps, it is found not only for benzene but also for toluene [26] and acetone [27] that the number of electrons per CO_2 molecule is higher than the overall number in the first sweep and lower in the subsequent ones. This means that in all these cases adsorbed intermediates are formed that are in a higher oxidation state than the educt.

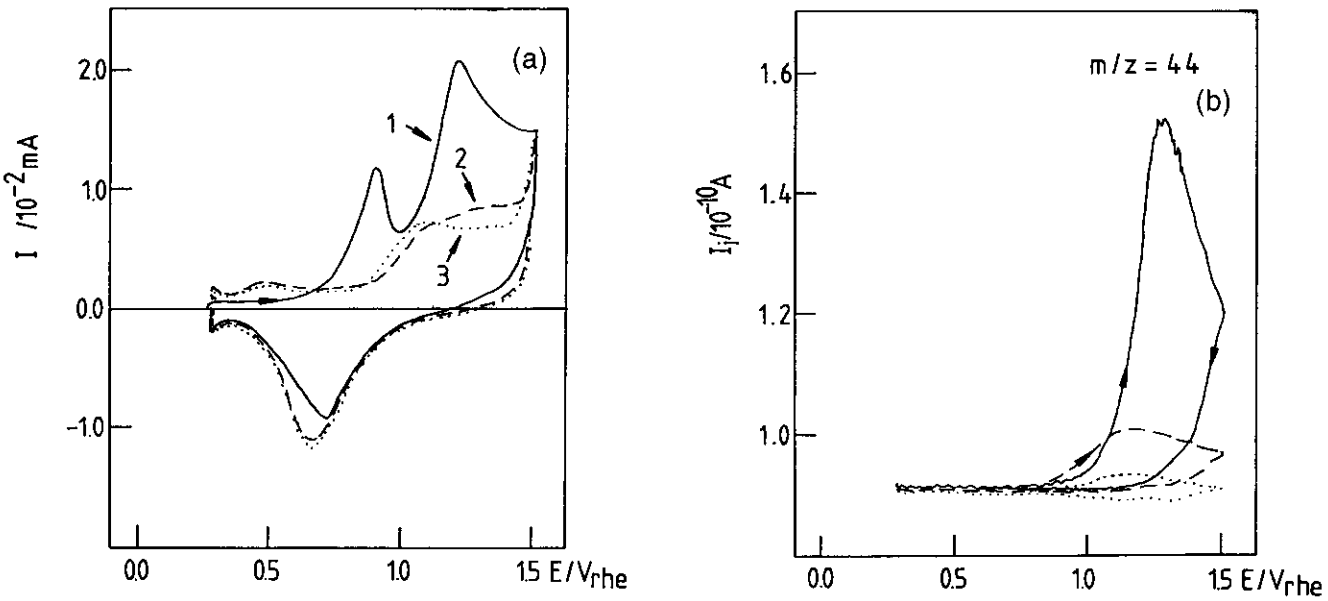

Figure 9 Oxidation of benzene preadsorbed on Pt(111). E_{ad}, 0.3 V; $c_{(benzene)}$, 2×10^{-4} M; v, 0.025 V/s, 0.05 M H_2SO_4. (a) Cyclic voltammetry, (b) mass spectrometric cyclic voltammogram (MSCV). (From Ref. 24.)

In many cases, desorption can also be induced by sweeping the potential in a negative direction after adsorption and electrolyte exchange. This is demonstrated again for benzene adsorbed on Pt(111) in Fig. 10. The negative potential limit of −50 mV is far in the hydrogen evolution region to make desorption as complete as possible. The cyclic voltammogram in the subsequent sweep has a form typical for Pt(111) in sulfuric acid and shows that desorption of benzene is nearly complete. The mass spectrometric cyclic voltammograms, which were recorded in parallel for m/z = 78 (benzene, Fig. 10b) and m/z = 84 (cyclohexane, Fig. 10c), show that benzene is desorbed at potentials below 150 mV and that cyclohexane is formed below 50 mV. Integrating the corresponding ion current and taking into account the different fragmentation probabilities for benzene and cyclohexane, it shows that on Pt(111) only one sixth of the adsorbate is hydrogenated, whereas the remaining part is desorbed as benzene.

This ratio is reversed when the experiment is performed with a roughened Pt(111) electrode, which is known to behave similar to a polycrystalline Pt electrode. Here, 15% of the adsorbate cannot be cathodically desorbed but are desorbed as CO_2 in a subsequent potential sweep into the oxygen adsorption region.Very similar is the behavior at the Pt(110) electrode, at which all adsorbed benzene is hydrogenated to cyclohexane. In none of the cases could another cathodic desorption product, such as cyclohexene or cyclohexadiene, be detected. Adsorbate coverages calculated (after calibration of the mass spectrometer for benzene, cyclohexane, and CO_2) from the sum of the integrated ion currents for desorbed benzene, cyclohexane, and the CO_2 formed during oxidation of the residual adsorbate in the subsequent positive sweep agree well (to within 15%) with that calculated when the adsorbate is directly oxidized to CO_2. In all cases, it is around 0.3 nmol/cm^2.

Again, this coverage agrees well with that found for benzene adsorbed on Pt(111) in UHV and suggests that the benzene molecule is adsorbed in a flat ("η_6") orientation. It also agrees with the Pt(111)-($\sqrt{21}*\sqrt{21}$)R10.9° benzene adlattice recently observed by scanning tunneling microscopy [28], for which the theoretical coverage is 0.34 nmol/cm^2.

It is obvious that hydrogenation only occurs at roughened surfaces or at the Pt(110) surface, which has a fairly open atomic structure. Only little or no hydrogenation occurs on Pt(111) or on Pt(100). Most probably the reason is the stabilization of a polar intermediate state during hydrogenation on the open surfaces, where the electron density is varying locally due to the Smoluchowski effect, which is missing on more densely packed surfaces. Another reason may be a weaker adsorption of benzene on Pt(111) and Pt(100), leading to desorption at a less low potential, where hydrogenation does not yet occur.

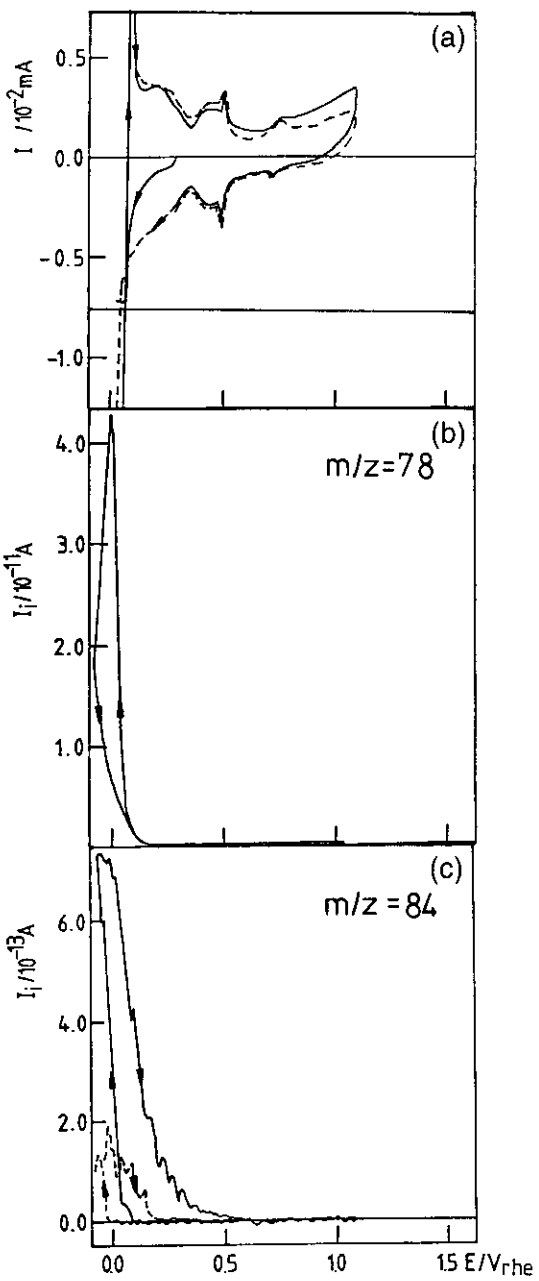

Figure 10 Cathodic desorption of preadsorbed benzene from Pt(111). (a) Cyclic voltammetry. (b) MSCV; m/z = 78 (benzene). (c) MSCV; m/z = 84 (cyclohexane). (From Ref. 24.)

More information can be obtained by using deuterated benzene. When adsorbing benzene-d_6 in light water on Pt(111) and desorbing it in the same electrolyte, the absence of an exchange of D-atoms by H (D/H exchange) in the desorbing benzene indicates that no C—D bond cleavage occurs.

This is different at Pt(100). Here, only one third of the adsorbed benzene is desorbed as such; the remainder stays on the surface even after extensive cycling to −100 mV and can only be oxidatively desorbed as CO_2. When using C_6D_6, most desorbed benzene is C_6D_6, but also other isotopic isomeres were observed, predominantly $C_6D_4H_2$ [25]. This points to the existence of an η_2-oriented adsorbate, which involves the cleavage of two C—H bonds. Such an η_2 orientation was postulated for hydroquinone and its derivates adsorbed on polycrystalline Pt on the basis of coverage data determined by the thin-layer electrode technique [29].

When doing similar experiments using Pt(110) or polycrystalline Pt, all or most of the adsorbate is hydrogenated. Using C_6D_6, desorption leads to $C_6H_2D_6$ as the predominant species (ca. 30%), but all isotopic isomers with a lower D content (down to C_6H_{12}) are also present. This can be understood if one assumes that during hydrogenation an intermediate is formed, which is in equilibrium with the educt: H/D exchange is possible in the reverse reaction of the preceeding equilibrium.

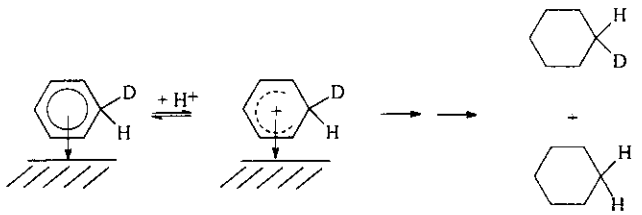

(14)

So far, however, the possibility cannot be excluded that the H/D exchange occurs during adsorption or in the adsorbed state. Here, displacement of the adsorbate in the double-layer region by another adsorbing species can give additional information. In the experiment depicted in Fig. 11, benzene adsorbed at 0.4 V was displaced still at the same constant potential from a porous polycrystalline electrode by introducing Cu^{2+} ions into the solution [30]. The cathodic current is due to the formation of the Cu–UPD layer; an ion current for m/z = 78 but not for m/z = 84 is detected. Integration shows that 70% of the adsorbate are displaced as benzene. Further desorption of benzene can be achieved when sweeping the potential in Cu-free solution in cathodic direction, as shown in Fig. 9. The amount of cyclohexane formed is still negligible, and only a small amount of carbonaceous species remains on the surface, as shown by the subsequent MSCV for CO_2 (the peak at 0.7 V in the CV corresponds to dissolution of Cu–UPD). The same experiment, using C_6D_6, shows that a D/H exchange takes place neither during adsorption nor in the adsorbed

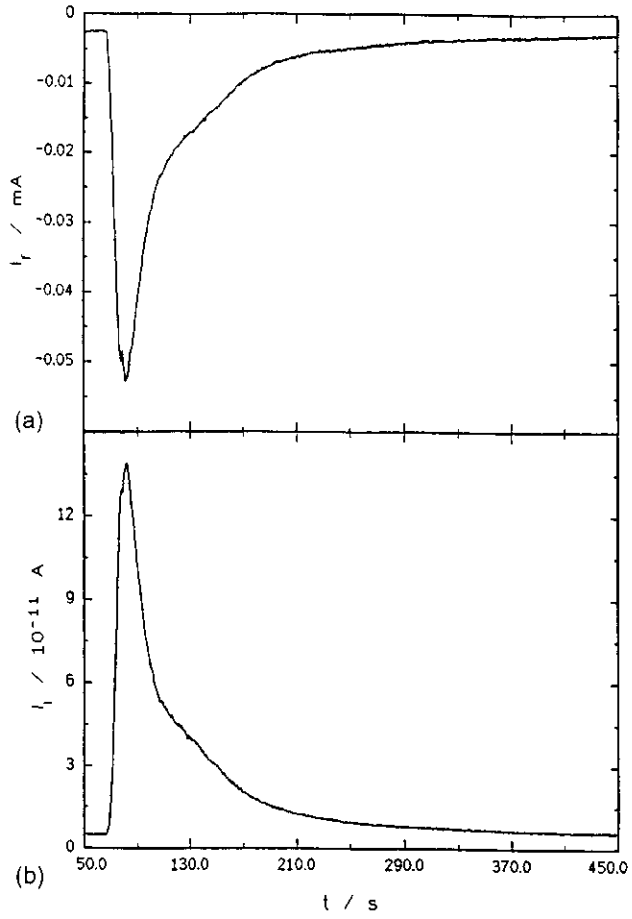

Figure 11 Displacement of benzene. (a) Current transient during Cu deposition onto polycrystalline Pt covered by preadsorbed benzene. E, 0.4 V; c(Cu^{2+}), 1 mM in 0.5 M H_2SO_4. (b) Ion current for benzene (m/z = 78). (From Ref. 28.)

state, confirming that the first step of the hydrogenation reaction is also responsible for the D/H exchange and therefore has to be reversible.

B. Cyclohexene

Another illustrative example for the use of this displacement technique is the adsorption of cyclohexene. In experiments involving potential sweeps into the hydrogen region, the adsorbate formed out of cyclohexene on Pt(110) is completely desorbed as cyclohexane. In the case of polycrystalline Pt, some benzene (~20%) is found in addition to cyclohexane. The adsorbate formed from cyclohexene therefore behaves similar to adsorbed benzene. This already suggests (but does not prove) that cyclohexene is dehydrogenated to benzene upon adsorption on these surfaces.

To verify this, cyclohexene was adsorbed on Pt(110) in the thin layer cell and, after electrolyte exchange and still under potential control, 10^{-4} M Cu^{2+} containing sulfuric acid was slowly introduced into the cell (cf. Fig. 5) at a flow rate of 0.2–0.05 μL/s. The flow rate has to be low enough for the desorbing species to reach the vacuum with a high probability, i.e., the residence time of the electrolyte in the thin-layer volume has to be high compared with the time constant of diffusion from the electrode to the Teflon membrane, which is approximately 2 s.

The only detectable species is benzene. As in the case of preadsorbed benzene, about one third of the adsorbate stays on the surface and is detected as CO_2 in a subsequent anodic sweep. However, despite the low flow rate, around 20% of the adsorbate is neither detected as benzene nor as CO_2 in the anodic sweep. This may not only be the case because benzene desorbing from the surface close to the outlet of the cell has no chance to reach the electrolyte vacuum interface but also because of edge effects. In a similar experiment, using the porous electrode in the conventional DEMS cell, at least 95% of the adsorbate is detected as benzene. Therefore, cyclohexene is dehydrogenated on polycrystalline Pt and Pt(110), indeed (cf. Fig. 12).

On Pt(111) the situation is different: Because the adsorbate formed on this surface is only desorbed as a minor volatile species, it is probably cyclohexanol, which is formed by addition of water to the double bound similar to the case of ethene (see below) [31].

C. Ethene

In UHV, ethene is probably one of the most often studied molecules. It has now been established that at low temperatures, ethene adsorbs as a di-σ-bound species on Pt(111) and Pt(110), which transforms to ethylidyne at about room temperature [32–35]. Attempts to study the adsorbate formed from ethene on Pt electrodes by Fourier transform infrared (FTIR) spectroscopy have, so far, not been successful (E. Pastor, personal communication, 1994).

On both Pt(111) [36] and Pt(110) [31], oxidation of the adsorbate formed from ethene starts at potentials only slightly positive of an adsorption potential of 0.3 V. Formation of CO_2, though, is retarded by at least 200 mV. This is similar to benzene adsorbed on Pt(111), although no such well-separated peaks can be distinguished; this means that oxidized intermediates are formed before being completely oxidized to CO_2. The number of electrons necessary for the formation of a CO_2 molecule out of the adsorbate decreases from 6 at an adsorption poten-

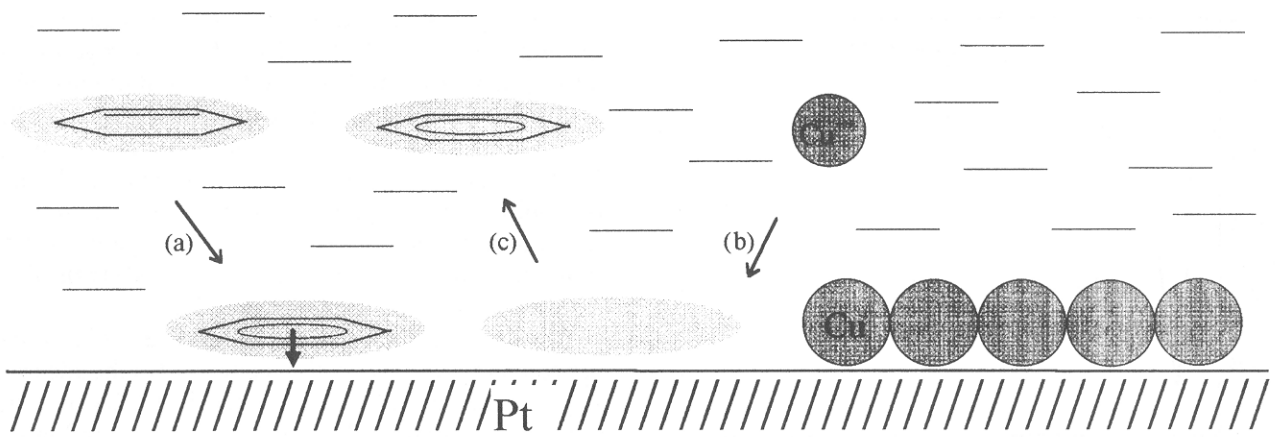

Figure 12 Illustration of the displacement process. (a) Adsorption of cyclohexene as benzene (b). (c) Displacement.

tial of 0.3 V to nearly 3 at an adsorption potential of 0.9 V, suggesting that at higher potentials adsorption proceeds oxidatively.

Again, more information on the adsorbed species is obtained from experiments in which the adsorbate is desorbed at low potentials, as demonstrated in Fig. 13 for a Pt(110) electrode. Ethane, butane, and methane (not shown) are formed. Experiments with C_2D_4 show that H/D exchange is nearly complete: Approximately 80% of the ethane and butane are d_0 species, and 20% are corresponding d_1 species.

Oxidation of the remaining adsorbate (Fig. 14) shows that parts of the adsorbate stay on the surface, half of which is oxidized in a peak at 0.7 V [37]. This is indicative of adsorbed CO, which is substantiated by comparing the amount of CO_2 formed in this peak to the corresponding oxidation charge, yielding an n_{ox} of two electrons per CO_2 molecule formed. Because such a well-defined oxidation peak, which is typical for adsorbed CO, is not present when the adsorbate is oxidized without preceeding cathodic desorption, we conclude that this CO is formed during the cathodic sweep. The formation of $C^{18}O^{16}O$ after adsorption in $H_2{}^{18}O$ proves that the adsorbate contains oxygen (Fig. 14).

Similarly, when the adsorbate is oxidized in $H_2{}^{18}O$ after adsorption in $H_2{}^{16}O$ without cathodic desorption, a significant amount of $C^{18}O^{16}O$ is formed below 0.8 V, largely exceeding the amount of $C^{18}O_2$. The oxygen-containing adsorbate might be formed by oxidative addition of water to the double bound:

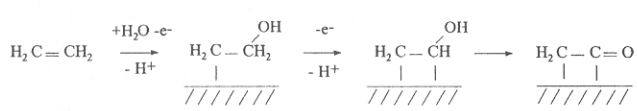

(15)

The results for different adsorption potentials are summarized in Fig. 15. The more positive the adsorption potential, the lower the overall amount of adsorbed species and the higher the amount of adsorbate, which can be desorbed as methane, and also the amount of adsorbed CO, except for 0.9 V, a potential at which this CO is directly oxidized to CO_2. The amount of methane is correlated to the amount of CO formed during the cathodic sweep, where CO is formed only although oxygen is present in the original adsorbate. Therefore, it is probable that an oxygen-containing C_2 adsorbate is formed, the amount of which increases with increasing potential and which decomposes at low potential to methane and adsorbed CO.

The reaction scheme in Fig. 16 summarizes the likely reactions and the structures of the adsorbate states. It seems clear from the results shown in Fig. 13 that besides the abovementioned oxygen-containing species, another adsorbate state is formed, leading to ethane, possibly di-σ-bound ethene $(C_2)^{\beta}$ and butane. Whether the dimerization occurs upon adsorption or upon cathodic desorption still has to be clarified.

All the adsorbates that cannot be cathodically desorbed belong to a third adsorbate state [$(C_2)^{\gamma}$-state], possibly ethydidyne, as known in UHV, but it is also possible that its molecular identity is not different from the previous one. The existence of a further fourth adsorbate state is revealed when trying to displace adsorbed ethene by other adsorbates. The using of I^-, CO, or Cu^{2+} leads to desorption of about 10% of the adsorbate as ethene [38]. It is tempting to assume that this state corresponds to a weakly π-bound species, recently observed in UHV [39].

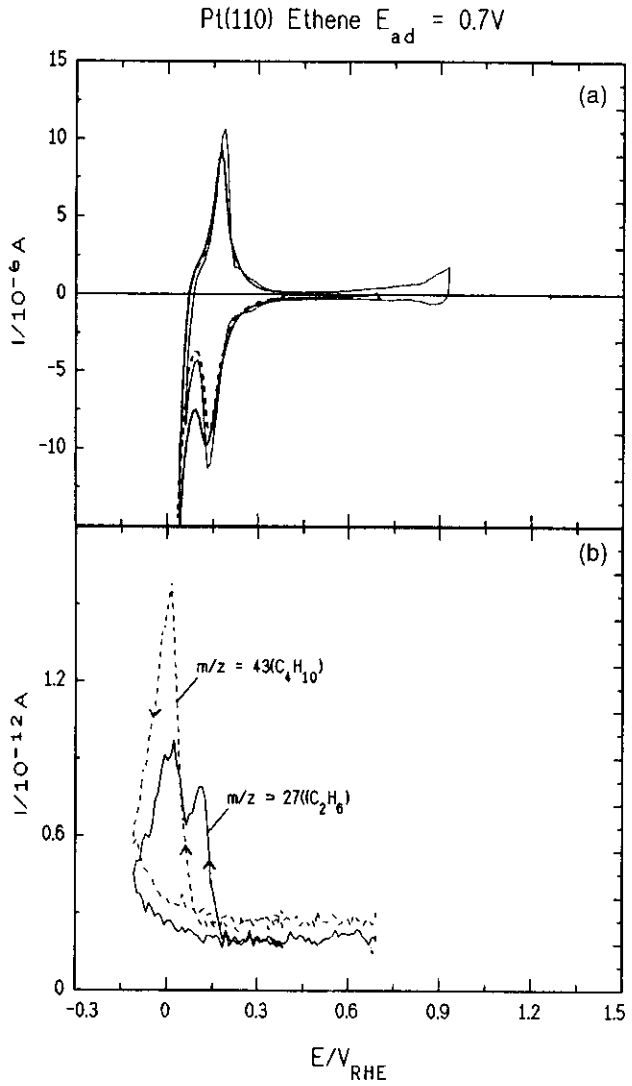

Figure 13 Cathodic desorption of preadsorbed ethene on Pt(110). E_{ad}, 0.7 V; c_{ethene}, 5.5×10^{-3} M; v, 12.5 mV/s, 0.1 M H_2SO_4. (a) Cyclic voltammetry: ——, first reduction sweep; - - - -, second reduction sweep; ——, sweep in the supporting electrolyte before adsorption. (b) MSCV: ——, m/z = 27 (ethane and butane); - - -, m/z = 43 (butane). (From Ref. 31.)

Similar adsorbate states exist on a Pt(111) electrode. However, cathodic desorption is less complete, and the $(C_2)^{\gamma}$ state is more abundant than on Pt(110).

D. Ethanol and Propanol

Studies of the adsorption and oxidation of ethanol are usually motivated by its possible use as a fuel in fuel cells. Here, as in the case of methanol, the adsorbate is believed to act as a catalyst poison; therefore, the conditions of

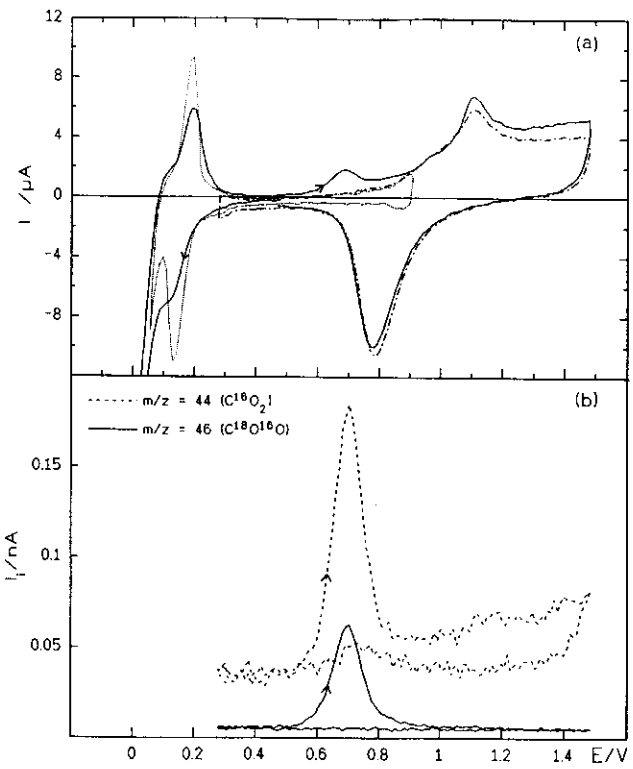

Figure 14 Oxidation of the cathodically nondesorbable adsorbate of preadsorbed ethene on Pt(110); adsorption in $H_2{}^{18}O/H_2SO_4$. Cathodic sweep and oxidation in $H_2{}^{16}O/H_2SO_4$. E_{ad}, 0.5 V; c_{ethene}, 5.5×10^{-4} M; v, 12.5 mV/s, 0.1 M H_2SO_4. (a) Cyclic voltammetry: ——, first sweep; - - -, sweep in the supporting electrolyte before adsorption; - · - · -, shape of the voltammogram after a few sweeps to 1.45 V. (b) MSCV for $C^{16}O_2$ and $C^{16}O^{18}O$. (From Ref. 37.)

the adsorbate formation and its possible reactions are of primary importance.

After adsorption at Pt(110) and after a subsequent electrolyte exchange at a constant potential of 0.3 V, methane desorbs during a potential sweep in a negative direction. This is seen in the MSCV for m/z = 15 (Fig. 17) [37]. On porous Pt and after adsorption from 0.1 M ethanol solution, also the desorption of ethane was observed [40]. Complete D/H exchange occurs in the formed methane; in the case of ethane, D/H exchange is only complete for the α-C atom, as shown by using CH_3 CD_2 OH in H_2O [41].

The residual adsorbate is oxidized mainly in a peak at 0.7 V, indicative of adsorbed CO, and in the oxygen adsorption region. The most straightforward interpretation would be that CO is formed from the COH group (i.e., the α-C atom), whereas methane originates from the methyl group.

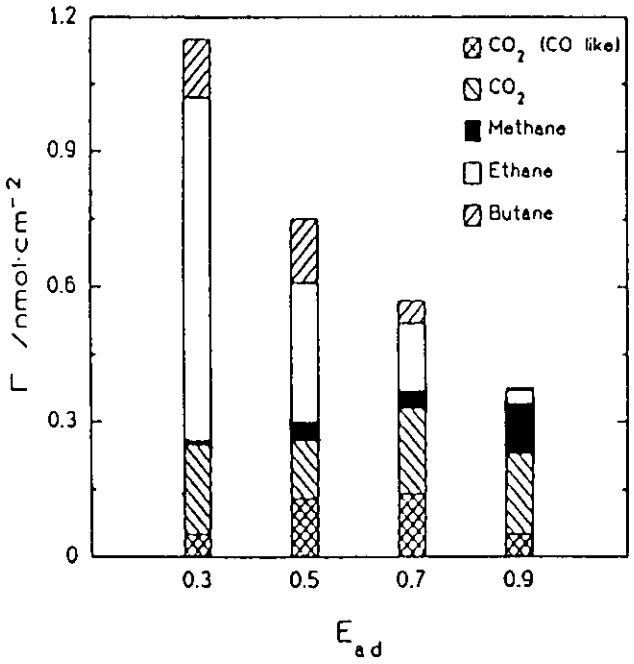

Figure 15 Desorption products of ethene on Pt(110). (From Ref. 31.)

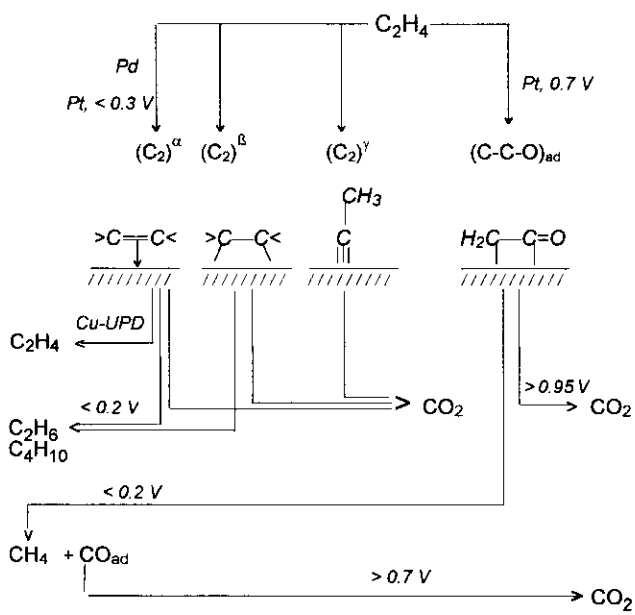

Figure 16 Surface reactions of ethene as suggested by DEMS (adsorbates in italics are hypothetical structures).

A closer inspection using $^{12}CH_3{}^{13}CH_2OH$, however, shows that the reactions are more complicated. Figure 18 shows the MSCV for $^{13}CO_2$ and $^{12}CO_2$ for the oxidation of the adsorbate with and without preceeding

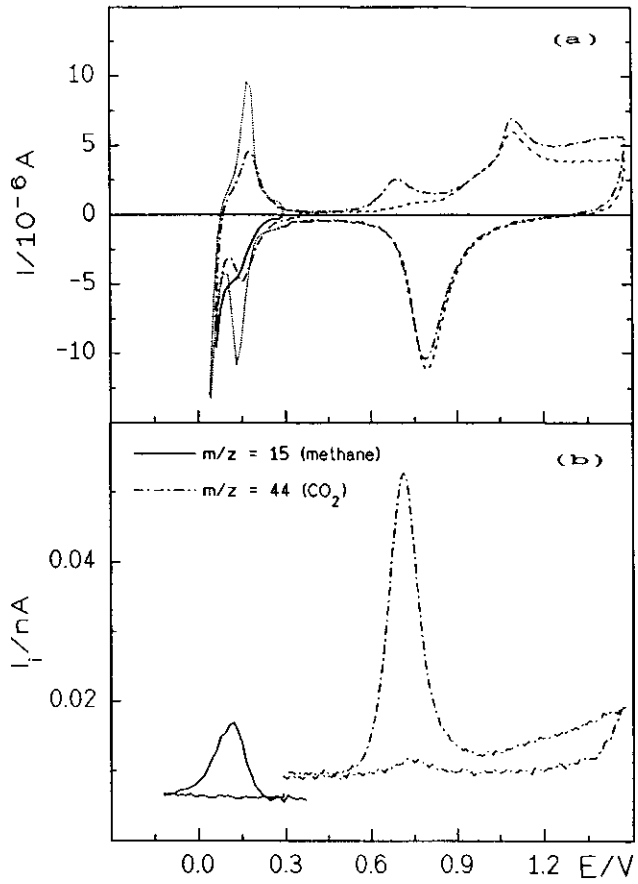

Figure 17 Cathodic desorption of preadsorbed ethanol from Pt(110) and subsequent oxidation of the remaining adsorbate. E_{ad}, 0.3 V; $c_{ethanol}$, 0.1 M; v, 0.0125 V/s, 0.1 M H_2SO_4. (a) Cyclic voltammetry: ————, first sweep in cathodic direction; · · · , subsequent oxidation; ···, Pt(110) in supporting electrolyte; – – – cyclic voltammetry after a few cycles between 0.06 and 1.45 V. (b) MSCV. (From Ref. 37.)

cathodic sweep. Obviously, a CO-like species is formed from both C atoms. Moreover, this experiment shows that only a part of the β-C atoms are cathodically desorbed. The amount of $^{13}CO_2$ decreases in both oxidation regions, whereas the amount of $^{12}CO_2$ is hardly affected. It is also informative to evaluate the number of electrons corresponding to the formation of one CO_2 molecule in the two oxidation regions. Whereas for the oxidation of adsorbed CO a value of $n_{ox} = 2$ is expected, the experimental value for the oxidation peak at 0.7 V is more than 4 without preceeding cathodic sweeps and still 3.4 after the desorption of methane. Therefore, other species than CO are oxidized at this potential. This is substantiated in an experiment, where the adsorption of ethanol

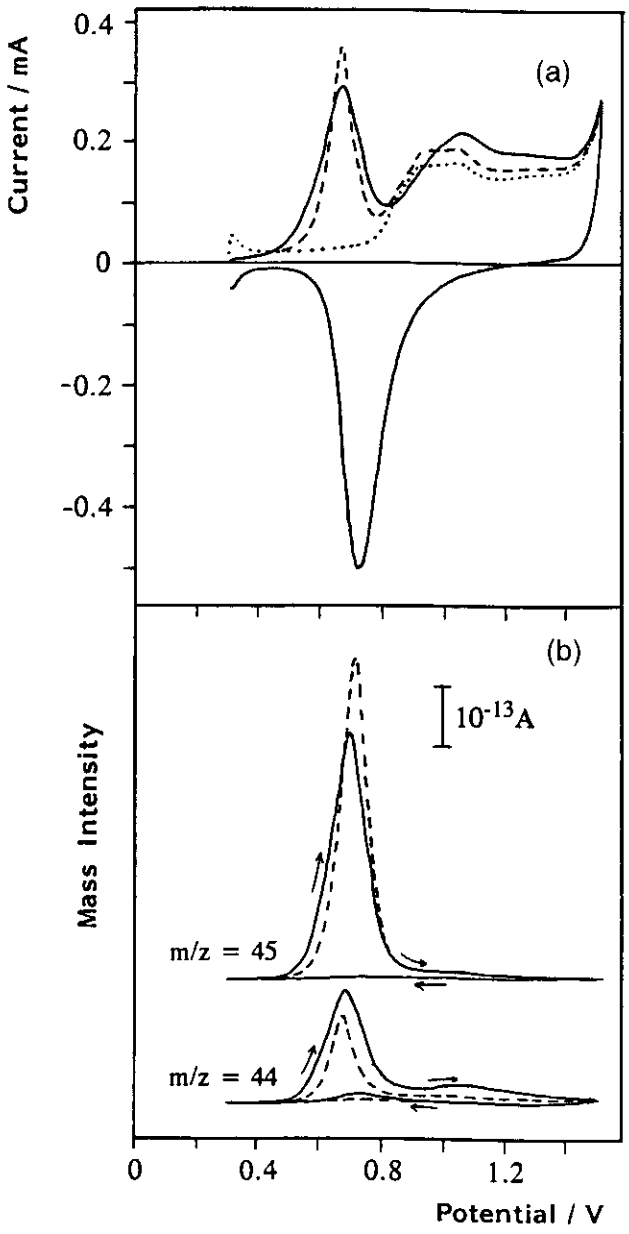

Figure 18 (a) Cyclic voltammogram of $^{12}CH_3{}^{13}CH_2OH$ adsorbates on sputtered Pt (real area, 10 cm^2) in 0.05 M H_2SO_4. E_{ad}, 0.30 V; sweep rate, 0.01 V/s. (b) Simultaneously recorded mass signal for m/z = 44 ($^{12}CO_2$) and 45 ($^{13}CO_2$). ——, direct electrooxidation; – – –, oxidation after the application of four cycles between 0.35 and 0.05 V; · · ·, Pt clean surface. (From Ref. 40.)

[42] and propanol [43] was performed in $H_2{}^{18}O$ and, afterwards the adsorbate was oxidized in $H_2{}^{16}O$. As shown in separate experiments, a complete exchange of OH takes place during the adsorption. In the peak at 0.7 V, both $C^{16}O^{18}O$ and $C^{16}O_2$ are formed, whereas in the oxygen adsorption region, only $C^{16}O_2$ was detected. Therefore, because no oxygen exchange occurs in adsorbed CO, also C atoms not yet bound to oxygen atoms are oxidized to CO_2 in the peak at 0.7 V. In the oxygen adsorption region, an n_{ox} of five to six electrons is obtained, as expected for CH_x species ($x = 1$–3). The results were very similar for Pt(110) and a polycrystalline Pt electrode [37].

The questions remain of what the actual nature of the adsorbate species is and whether the C—C bond cleavage already occurs during adsorption or during the cathodic sweeps. Other techniques have to be used to gain additional information. With FTIR spectroscopy, it was possible to exclude the presence of adsorbed CH_3 or CH_2 species [40]. Instead, it was suggested that =COH—CH_3, —OCH_2 CH_3, —CO—CH_3, and CO were present on the surface; CO would be formed simultaneously to methane even at an adsorption potential of 0.3 V, which is close to that where CH_4 formation starts in the cathodic sweep.

The possibility of splitting the C—C bond electrocatalytically is of primary importance for the use of ethanol in fuel cells, where a complete combustion is necessary. Figure 19 shows the cyclic voltammetry and the MSCV in an ethanol-containing electrolyte: to distinguish between the oxidation products CO_2 and CH_3CHO (ethanal), ethanol-d_5 was used here [44]. In the anodic sweep, the ion intensity for CO_2 is larger than that for ethanal; however, the true ratio of the two species has not been evaluated. Because of the higher solubility of ethanal in water, a larger part of this product remains in the aqueous phase. In the cathodic sweep, the amount of ethanal is much larger than that of CO_2. Thus, ethanal is the main oxidation product during ethanol oxidation and the C—C bond cleavage, leading to CO_2 only occurs to a minor extent. Formation of CO_2 in the anodic sweep is probably mainly due to oxidation of the adsorbed species. Because some CO_2 is formed during the cathodic sweep, there is the possibility of a C—C bond cleavage during a continuous oxidation. Using a direct methanol fuel cell at 175°C and direct mass spectrometric detection of products. Wang et al. [45] found up to 40% CO_2, besides 60% ethanal. This ratio was hardly influenced by using a Pt–Ru alloy [45]. Similar experiments have been performed with 1-propanol [43,46]. 1-Propanal is the main oxidation product formed above 0.4 V. Above 0.7 V propionic acid is also formed as detected by FTIR. Cathodic desorption of preadsorbed 1-propanol leads to formation of ethane and propane.

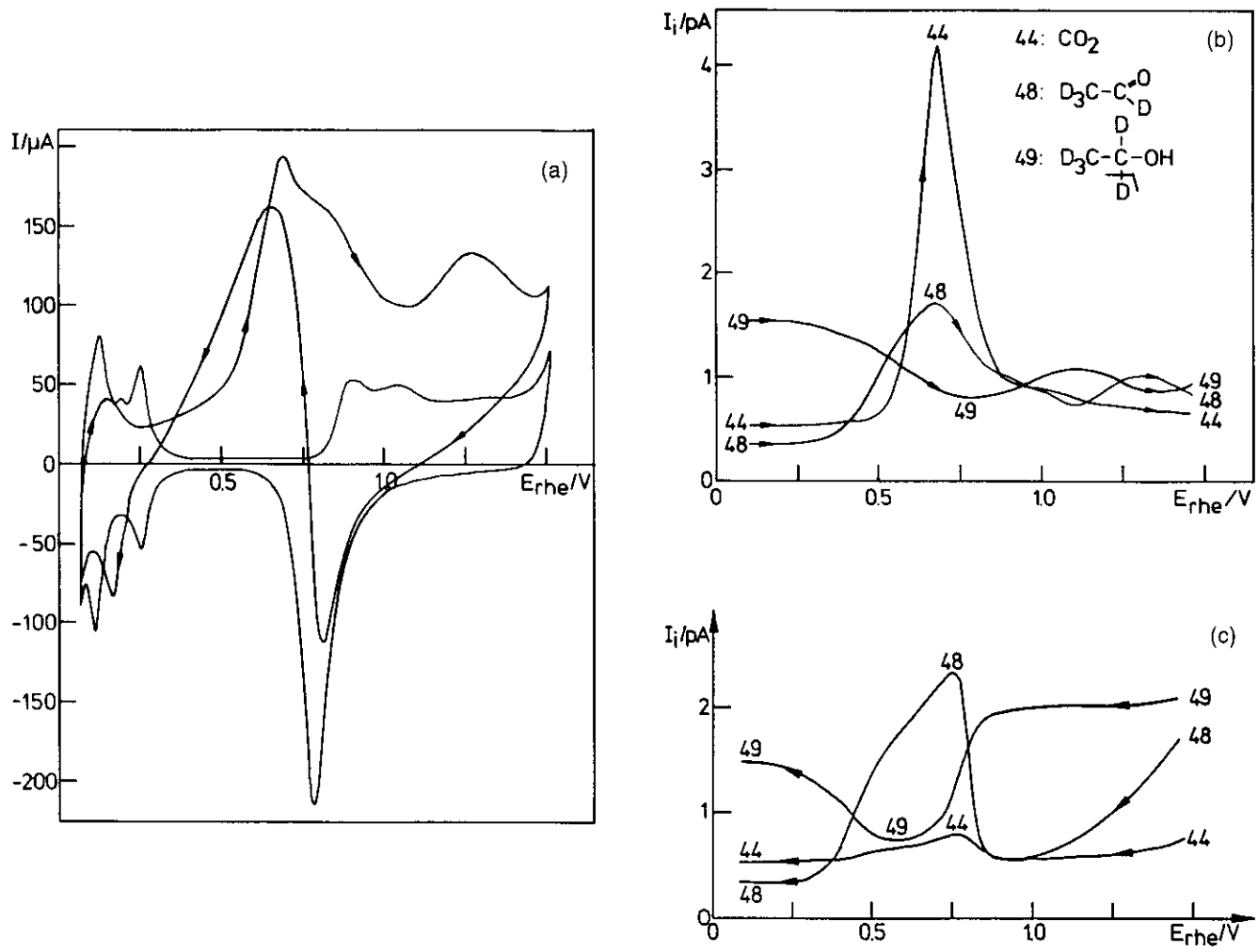

Figure 19 Oxidation of ethanol on a porous Pt-lacquer electrode (10^{-2} M ethanol in 0.5 M H_2SO_4, v, 3.1 mV/s) [42,44]. (a) Cyclic voltammetry (thin line without arrows: supporting electrolyte). (b) MSCV for the ions as indicated, anodic sweep with ethanol-d_5 in solution. (c) Same as (b), cathodic sweep. (From Ref. 44.)

E. Other Organic Adsorbates on Pt

Of primary importance in fuel cell research is the adsorbate formed from C_1 compounds, which acts as a catalyst poison. It is now generally accepted that this species is CO. Except for confirming the identity of this species by evaluating the number of electrons necessary for oxidation to CO_2, DEMS is superior to simply using cyclic voltammetry in elucidating the onset potential of oxidation and coverages, especially when using less noble catalysts or bimetallic catalysts, because of the appreciable pseudocapacitive currents on those surfaces. The same is true for the adsorbate directly formed out of CO, which is present in the H_2 formed in methanol reformers; for Pt–Ru catalysts pseudocapacitive currents have been shown to amount to 50% of the overall oxidation charge [20].

In addition, halogenated methanes and 1,1,1, trichloroethane and tetrachloroethene have been studied by DEMS [47,48]. Astonishingly, all of the adsorbates formed behave in a very similar way: cathodic desorption leads to methane and ethane and, in the case of tetrachloroethene compounds, also to propane. Therefore, in all of these cases CH_n (with $n \approx 2$) fragments seem to be formed, involving a C—C bond cleavage in the case of tetrachloroethene. Adsorption of

trichloroethane accordingly leads to species desorbing as ethane and propane. H/D exchange is appreciable. In addition, an adsorbate behaving like adsorbed CO is formed.

Results achieved by DEMS clearly show that many organic species form a variety of adsorbate states. This has also been shown for acetonitrile [49], dimethylsulfoxide, and sulfolane [50]. In the case of acetonitrile it is particularly interesting that a part of the adsorbate formed at Pt in the double-layer region is desorbed at more anodic potentials without being oxidized, similar to benzene adsorbed on Rh or Pd (see below). Oxidation of nitrogen-containing organic adsorbates not only leads to CO_2 but also nitrogen oxide and, in the case of adsorbed aniline, to HCN [51].

The high sensitivity of DEMS is demonstrated by the fact that even desorption products of biphenyl, desorbing as biphenyl from a Pt(111) electrode, and naphtalene, desorbing as naphtalene and as the partially hydrogenated tetralin, were detected [52].

F. Adsorbates on Less Noble Electrodes

Organic adsorbates are often used as inhibitors of corrosion or as brighteners in metal plating. Fundamental studies of the adsorption on these less noble metals, like Cu, Ni, or Fe, are much more difficult. Metals like Pd and Rh can serve as model electrodes, because the normal potential of the corresponding metal electrodes is in between that of Pt or Au and the above mentioned metals.

In Fig. 20, the cyclic voltammetry and MSCV of a polycrystalline Rh electrode with preadsorbed benzene in sulfuric acid is shown [51]. A part of the adsorbate is desorbed cathodically as benzene or cyclohexane, but a significant part is also desorbed as benzene during the subsequent anodic sweep at potentials where oxygen adsorbs. Only a part of the adsorbate is oxidized to CO_2. Note that an appreciable amount of CO_2 is formed out of the adsorbate during the cathodic sweep at potentials where adsorbed oxygen is reduced, indicating the necessity of a partially uncovered surface for the oxidation reaction.

Similarly, when CO is adsorbed on an Ni electrode and the potential is changed to more positive values, only a part is oxidized to CO_2 and the other part is desorbed as CO, the relative amounts depending on the pH [53].

IV. FARADAIC ORGANIC REACTIONS

The hydrogenation reactions described in the previous sections are reactions of species previously adsorbed, usually at a different potential. From these, the continu-

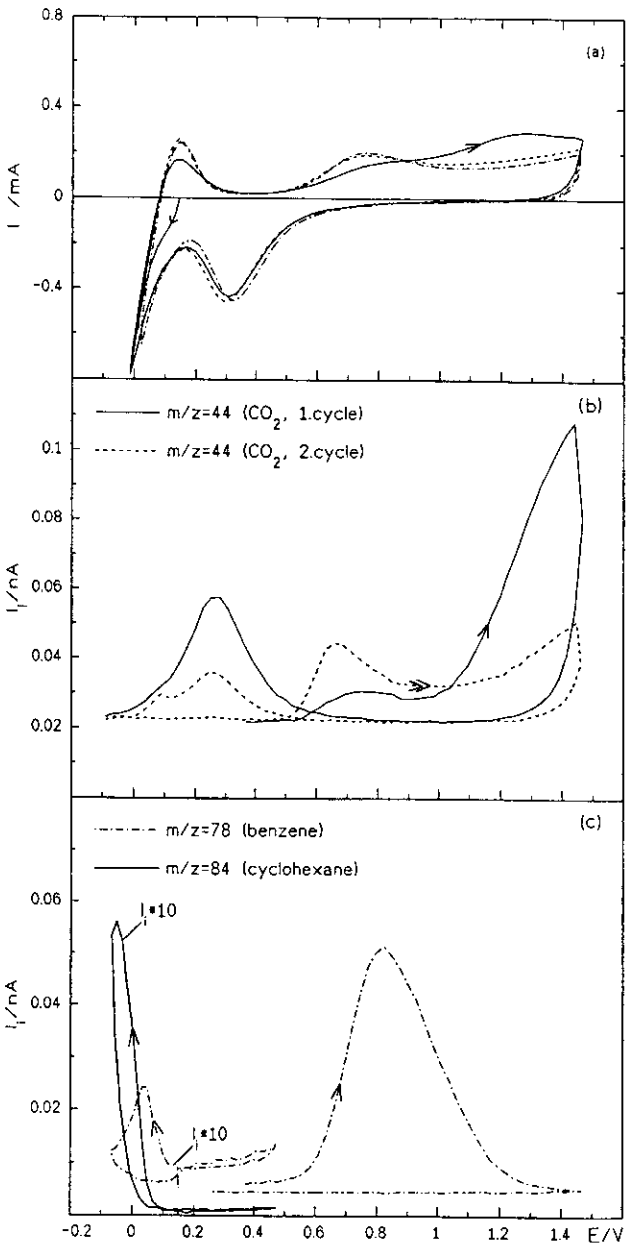

Figure 20 Cathodic desorption of preadsorbed benzene and subsequent oxidation of the remaining adsorbate at polycrystalline rhodium. E_{ad}, 0.15 V; v, 25 mV/s, 0.5 M H_2SO_4; $c_{benzene}$, 2×10^{-2} M. (a) Cyclic voltammetry: ——, first cycle (initial cathodic direction); – – –, second cycle; –·–·–, in supporting electrolyte. (b and c) MSCV. Below 0.1 V, the ion currents of cyclohexane and benzene are enlarged by a factor of 10. (From Ref. 51.)

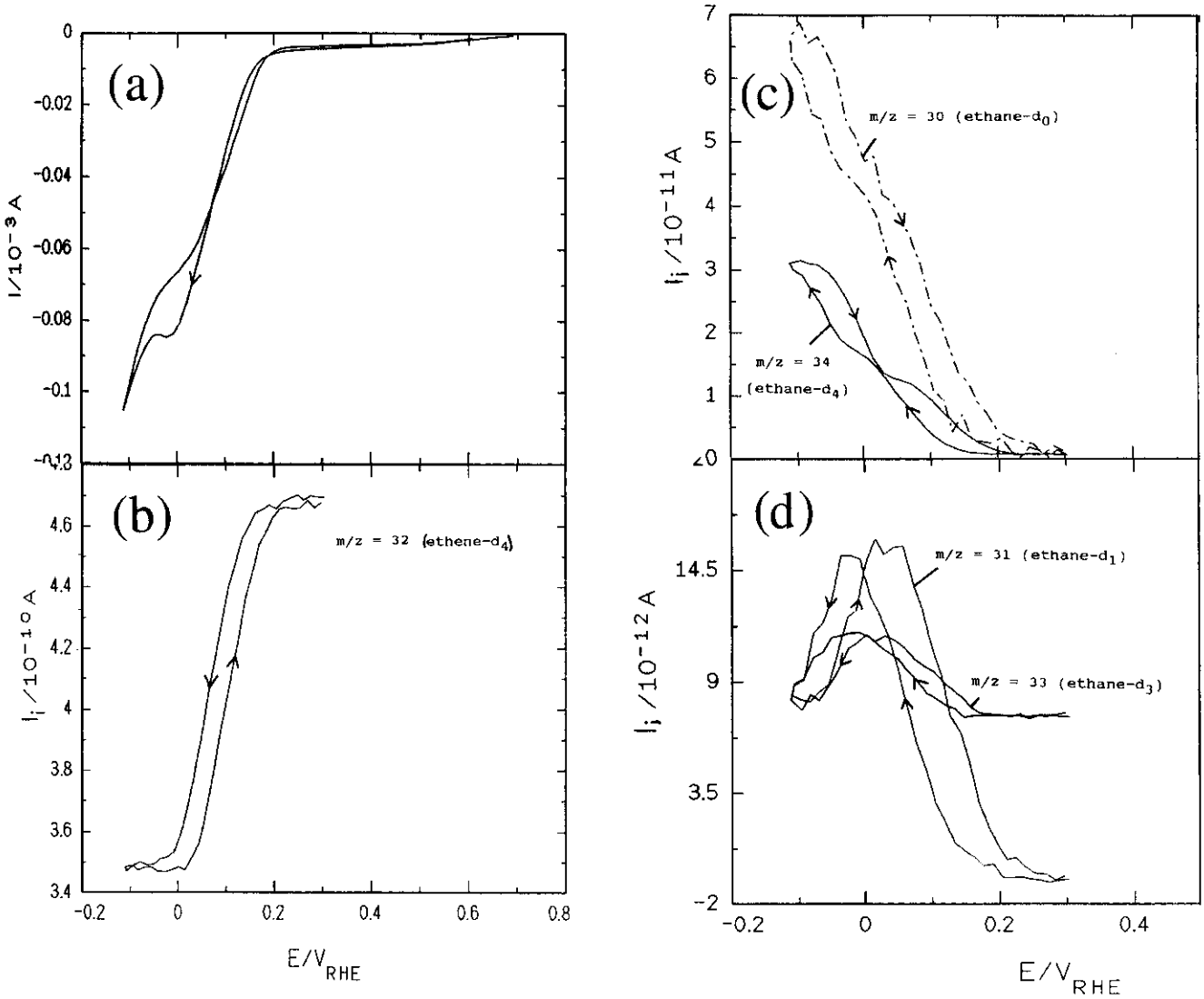

Figure 21 Bulk hydrogenation of ethene-d_4 at Pt(110). (a) Cyclic voltammetry in 0.1 M H_2SO_4; flow rate $u = 0.45$ μL/s; scan rate $v = 12.5$ mV/s. (b) Decrease of educt signal ethene-d_4 (5.5×10^{-4} M) (m/z = 32). (c) Increase of product signals: ——, m/z = 34 (ethane-d_4); – · – · –, m/z = 30 (ethane-d_0). (d) Increase of product signals: ——, m/z = 33 (ethane-d_3); and m/z = 31 (ethane-d_1). (From Ref. 16.)

ous reaction of species from the bulk has to be distinguished. Here, adsorbed intermediates may be formed, but this occurs at the same potential as the continuous reaction; moreover, their surface concentration may be very low. Such intermediates therefore may but do not have to be different from those preadsorbed species. To distinguish reactions of an adsorbate accumulated on the surface and the "bulk" reaction, it is advantageous to work under conditions of constant mass transport, e.g., by using a constant flow of electrolyte in the thin-layer cells (cf. Fig. 5 or 6) or by using forced convection.

A. Continuous (Bulk) Hydrogenation

The hydrogenation of most of the unsaturated species mentioned above has also been studied by DEMS. It usually leads to the formation of the alkane correspond-

ing to the carbon skeleton. The influence of the surface structure of Pt electrodes on the hydrogenation has been studied for ethene [16], ethine [21], and cyclohexene [31]. As for desorption reactions, the Pt(110) surface or roughened surfaces are much more active than the Pt(111) surface. Hydrogenation of ethene and acetone [27] in deuterated electrolyte(on using the deuterated compound in light water) results in a broad distribution of the isotopic isomeres formed (cf. Fig. 21). Because hydrogenation of the preadsorbed species results in a nearly complete H/D exchange (e.g., adsorbed C_2D_4 is hydrogenated to C_2H_6), the residence time in the adsorbed state, where the H/D exchange is occuring, is comparable with the overall hydrogenation rate. According to the reaction sequence of Eq. (16), obviously the first step of hydrogenation (after adsorption) is reversible and occurs at a rate comparable with the final hydrogenation and desorption step. (If the addition of the first proton is fast, i.e., if this reaction is in equilibrium, complete H/D exchange should occur. If the final step is fast compared with the first one, no H/D exchange can occur.)

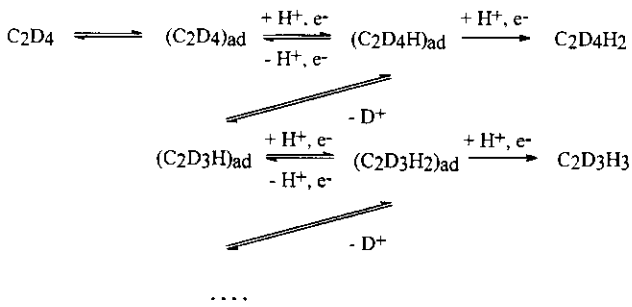

(16)

B. Reactions on Ib Metals

In the case of Au, Ag, and Cu, adsorption of most organic species is much weaker than on Pt; therefore, most DEMS studies deal with faradaic reactions.

1. Unsaturated Hydrocarbons on Au

Ethene is oxidized on Au in sulfuric acid to CO_2, acetaldehyde, and acetic acid, which was identified by FTIR [54,55]. Propene has been shown to yield acetone, acetaldehyde, and CO_2 upon oxidation [56]. Allyl alcohol and propargyl alcohol are oxidized to CO_2 and acrolein or propargylaldehyde; respectively, propargyl alcohol can be reduced to propene, propine, and allyl alcohol [57]. Only ethine and propargyl alcohol form strongly bound adsorbates.

2. Reduction of CO_2

Copper is known to be a good catalyst for reduction of CO_2. In carbonate solutions, however, a variety of products are formed. DEMS is ideally suited to study the relative amounts of the volatile products, mainly methane and ethene, as a function of electrolyte composition, etc. [22,58]

3. Hydrogen Evolution During Formaldehyde Oxidation

Probably one of the most puzzling electrochemical reactions, which is also of great technological importance in currentless metal deposition, is the hydrogen evolution during formaldehyde oxidation at Ib metal electrodes and at potentials very positive to the reverse hydrogen evolution potential. It has been known for a long time that this reaction proceeds via the overall equation

$$2HCHO + 4OH^- \rightarrow 2HCOO^- + 2H_2O + H_2 + 2e^-$$

Using DEMS, this has been verified by Jusys and Vaskelis [59–62], who have also studied the kinetic isotope effect and who, by using isotopic isomers, verified that the evalved hydrogen solely originates from the formaldehyde molecule and not from water. When using a mixture of HCHO and DCDO, not only H_2 and D_2 but also HD are formed; therefore, both atoms in the hydrogen molecule originate from separate formaldehyde molecules, which is only possible if hydrogen atoms are adsorbed on these electrodes [63]. It is clear that H_2 molecules are not oxidized at positive potentials at Ib metals because their dissociation is not possible at these surfaces. It is, however, astonishing that adsorbed H atoms are not oxidized either but desorbed as H_2.

V. INORGANIC REACTIONS

Besides carbon, the element with the largest number of abundant volatile compounds is nitrogen. Reaction of nitrogen compounds are therefore well suited for being studied by DEMS. Among these are NO_2^- [64,65], leading to NO_2 upon oxidation and N_2O upon reduction, and NH_2OH [64], leading to a variety of oxidation products. The reduction of NO was also studied on Au single-crystal electrodes [66]. N_3^- is oxidized to N_2, NO, NO_2, and N_2O on Au and Pt electrodes. Only on Pt electrodes it is also reduced, leading to N_2, N_2H_4, and possibly NH_3 [67].

Using ^{18}O-tracers, it has been shown that no oxygen exchange occurs during O_2 evolution at Pt oxide [68] but at RuO_2 [69]. Interestingly, even the formation of RuO_4 could be observed mass spectrometrically. Further

studies of other elements involve the reduction of As, deposited on Au, to AsH_3 (A. Dülberg and H. Baltruschat, unpublished data 1991), the photocatalytic oxygen and chlorine evolution at TiO_2 electrodes [70], and the photocatalytic corrosion of InP single-crystal electrodes to PH_3 [23].

VI. CONCLUDING REMARKS

We showed here that DEMS can be used for both on-line detection of electrochemical reaction products and the study of adsorbates. Reaction and desorption products can be determined semiquantitatively. Because in many cases several products are formed, it is important to know their amounts to distinguish between the main and side reactions.

As to the detection of electrochemical reaction products, it has the advantage over other methods, e.g., chromatography, of being fast and highly sensitive. Amounts below 1 nmol can be easily detected. Thus, it is ideally suited for studying reactions at single-crystal electrodes with their limited overall surface area; besides, the maximum time of reaction at single crystals is limited due to their possible deterioration by contaminants. In comparison with FTIR spectroscopy, DEMS has the advantage of an easier potential control, because the thin layer is 50–100 μm thick instead of only (ill-defined) 1 μm. The disadvantage of course is that only volatile products can be detected.

For the study of organic adsorbates, FTIR spectroscopy again is the technique most often used besides DEMS. Both techniques yield complementary information. Different adsorbate states and their reactions can be identified semiquantitatively by DEMS (including their oxidation states). Additional information about the binding geometry and elementary composition can often be obtained using isotopically labeled compounds. For elucidation of the exact nature of the adsorbate, a spectroscopic method like FTIR has to be used (see Chapter 21). The sole use of such a method, however, is not able to yield complete information because only adsorbates with a vibrational dipole to the surface can be detected and because it is not quantitative. For such (semi-) quantitative measurements, DEMS is a powerful technique.

ACKNOWLEDGMENT

Thanks are due to the Deutsche Forschungsgemeinschaft for generous financial support.

REFERENCES

1. JL Falconer, JA Schwarz. Catal Rev Sci Eng 25:141–227, 1983.
2. A Cassuto, DA King. Surf Sci 102:338, 1981.
3. RR Bruckenstein, J Gadde. J Am Chem Soc 93:793, 1971.
4. O Wolter, J Heitbaum. Ber Bunsenges Phys Chem 88:2–6, 1984.
5. O Wolter, J Heitbaum. Ber Bunsenges Phys Chem 88:6–10, 1984.
6. T Kotiaho, FR Lauritsen, TK Choudhury, RG Cooks. Anal Chem 63:875A–883A, 1991.
7. B Bittins-Cattaneo, E Cattaneo, P Königshoven, W Vielstich. In: AJ Bard, ed. Electroanalytical Chemistry, A Series of Advances. Vol. 17. New York: Marcel Dekker, 1991, pp. 181–220.
8. G Eggert, J Heitbaum. Electrochim Acta 31:1443–1448, 1986.
9. C-P Maschmeier, H Baltruschat. Electrochim Acta 37:759–761, 1992.
10. R Ianniello, VM Schmidt. Ber Bunsenges Phys Chem 99:83–86, 1995.
11. J Willsau, J Heitbaum. Electrochim Acta 31:943–948, 1986.
12. J Clavilier, R Albalat, R Gomez, JM Orts, JM Feliu, A Aldaz. J Electroanal Chem 330:489–497, 1992.
13. A Dülberg. Die Adsorption und Zersetzung halogenierter Kohlenwasserstoffe an Elektrokatalysatoren, Untersuchungen mit elektrochemischer Massenspektrometrie. Dissertation, Universität Witten-Herdecke, Witten-Herdecke, 1994.
14. D Tegtmeyer, A Heindrichs, J Heitbaum. Ber Bunsenges Phys Chem 93:201–206, 1989.
15. M Fujihira, T Noguchi. J Electroanal Chem 347:457–463, 1993.
16. H Baltruschat, U Schmiemann. Ber Bunsenges Phys Chem 97:452–460, 1993.
17. T Hartung, H Baltruschat. Langmuir 6:953 957, 1990.
18. U Schmiemann. Der Einfluß der Struktur von Edelmetalloberflächen auf die Elektrosorption organischer Moleküle, Untersuchungen mit differentieller elektrochemischer Massenspektrometrie. Dissertation, Universitä Witten-Herdecke, Witten-Herdecke, 1993.
19. U Müller. DEMS-Studie zum elektrochemischen Reaktionsverhalten ungesättigter Kohlenwasserstoffe an Platin-Einkristalloberflächen sowie an polykristallinen Platin- und Palladium-Elektroden. Dissertation, Universität Witten-Herdecke, Witten-Herdecke, 1996.
20. Z Jusys, H Massong, H Baltruschat. J Electrochem Soc 146 (1999, in press).
21. Y Gao, H Tsuji, H Hattori, H Kita. J Electroanal Chem 372:195–200, 1994.
22. S Wasmus, E Cattaneo, W Vielstich. Electrochim Acta 35:771–775, 1990.
23. P Bogdanoff, P Friebe, P Alonso-Vante. J Electrochem Soc 145:576–582, 1998.

24. T Hartung, U Schmiemann, I Kamphausen, H Baltruschat. Anal Chem 63:44–48, 1991.
25. U Schmiemann, H Baltruschat. J Electroanal Chem 347:93–109, 1993.
26. JM Zhu, T Hartung, D Tegtmeyer, H Baltruschat, J Heitbaum. J Electroanal Chem 244:273–286, 1988.
27. B Bänsch, T Hartung, H Baltruschat, J Heitbaum. J Electroanal Chem 259:207–215, 1989.
28. S-L Yau, Y-G Kim, K Itaya. In situ STM of benzene chemisorbed on Rh(111) and Pt(111) in hydrofluoric acid. Sixth International Symposium on Electrode Processes, Los Angeles, CA, 1996, pp. 243–256.
29. MP Soriaga, AT Hubbard. J Am Chem Soc 104:2742, 1982.
30. U Müller, A Stoyanova, H Baltruschat. Displacement of adsorbed benzene by Cu-UPD: a DEMS-study at polycrystalline Pt and Pt(110)-electrodes. Sixth International Symposium on Electrode Processes, Los Angeles, CA, 1996, pp. 257–268.
31. U Müller, U Schmiemann, A Dülberg, H Baltruschat. Surf Sci 335:333–342, 1995.
32. MM A Cassuto, J Jupille. Surf Sci 249:8, 1991.
33. F Zaera. J Am Chem Soc 111:4240, 1989.
34. RIM E Yagasaki. Surf Sci 64:157, 1977.
35. WTT L Ping Wang, RM Ormerod, RM Lambert, H Hoffmann, F Zaera. J Phys Chem 94:4236, 1990.
36. U Schmiemann, H Baltruschat. J Electroanal Chem 340:357–363, 1992.
37. U Schmiemann, U Müller, H Baltruschat. Electrochim Acta 40:99–107, 1995.
38. U Müller, A Dülberg, H Baltruschat. Colloids Surf A 134:155–164, 1998.
39. H Öfner, J Zaera. J Phys Chem B 101:396, 1997.
40. T Iwasita, E Pastor. Electrochim Acta 39:531–537, 1994.
41. E Pastor, T Iwasita. Electrochim Acta 39:547–552, 1994.
42. J Willsau, J Heitbaum. J Electroanal Chem 194:27–35, 1985.
43. T Hartung. Adsorption und Desorption von Benzol und aliphatischen Brennstoffen auf glattem Platin und Platin(111): Eine Untersuchung mit differentieller elektrochemischer Massenspektrometrie (DEMS). Dissertation, Universität Witten-Herdecke, Witten-Herdecke, 1989.
44. J Willsau. Zur Elektrochemie kleiner Moleküle, Aufklärung der Elementarschritte durch Kombination von DEMS und Isotopenmarkierung. Dissertation, Universität Bonn, Bonn, 1985.
45. J Wang, S Wasmus, RF Savinell. J Electrochem Soc 142:4218–4224, 1995.
46. E Pastor, S Wasmus, T Iwasita, MC Arèvalo, S Gonzàlez, AJ Arvia. J Electroanal Chem 350:97–116, 1993.
47. H Baltruschat, M Beltowska-Brzezinska, A Dülberg. Electrochim Acta 38:281–284, 1993.
48. U Müller, A Dülberg, A Stoyanova, H Baltruschat. Electrochim Acta 42:2499–2509, 1997.
49. S Wasmus, W Vielstich. J Electroanal Chem 345:323–335, 1993.
50. S Wasmus, W Vielstich. Electrochim Acta 38:175–183, 1993.
51. U Schmiemann, Z Jusys, H Baltruschat. Electrochim Acta 39:561–576, 1994.
52. J Vrestal, T Löffler, U Müller, H Baltruschat. J Electroanal Chem 1998.
53. CF Zinola, EJ Vasini, U Müller, H Baltruschat, AJ Arvia. J Electroanal Chem 415:165–167, 1996.
54. G Semrau, J Heitbaum. Electrochemical reactions of ethene on Pt and Au in sulfuric acid. Meeting of Electrochemical Society, San Francisco, CA, 1984, p. 639.
55. VM Schmidt, E Pastor. J Electroanal Chem 376:65, 1994.
56. VM Schmidt, E Pastor. J Electroanal Chem 401:155–161, 1996.
57. E Pastor, VM Schmidt, T Iwasita, MC Arevalo, S Gonzalez, AJ Arvia. Electrochim Acta 38:1337–1344, 1993.
58. P Friebe, P Bogdanoff, N Alonso-Vante, H Tributsch. J Catal 168:374–385, 1997.
59. Z Jusys, A Vaskelis. Electrochim Acta 42:449–454, 1997.
60. Z Jusys. J Electroanal Chem 375:257–262, 1994.
61. Z Jusys, A Vaskelis. Langmuir 8:1230–1231, 1992.
62. Z Jusys, A Vaskelis. J Electroanal Chem 335:93–104, 1992.
63. NA Anastasijevic, H Baltruschat, J Heitbaum. Electrochim Acta 38:1067–1072, 1993.
64. P Karabinas, O Wolter, J Heitbaum. Ber Bunsenges Phys Chem 88:1191–1196, 1984.
65. S Wasmus, E Vasini, M Krausa, H Mishima, W Vielstich. Electrochim Acta 39:23–31, 1994.
66. S Suzuki, T Nakato, H Hattori, H Kita. J Electroanal Chem 396:143–150, 1995.
67. A Dalmia, S Wasmus, RF Savinell, CC Liu. J Electrochem Soc 142:3735–3740, 1995.
68. J Willsau, O Wolter, J Heitbaum. J Electroanal Chem 195:299–306, 1985.
69. M Wohlfahrt-Mehrens, J Heitbaum. J Electroanal Chem 237:251–260, 1987.
70. P Bogdanoff, N Alonso-Vante. Ber Bunsenges Phys Chem 97:940–942, 1993.